III A. Neutrino Beam Design and Construction

It is desirable to tune the energy spectrum of the neutrino beam to maximize the likelihood of observing an oscillation signal. This amounts to using neutrinos whose energy spectrum is largely confined between 0.5 and 1.5 GeV. The technique we plan to use to produce such a beam [1] is discussed in detail in this chapter (section III.1.1).

At the same time, because the experiment has a long baseline, it is essential that steps be taken to maximize the neutrino flux. To accomplish this goal, the AGS proton intensity needs to be high, the targeting efficient, pion focusing optimized, and the pion decay space long. Since it is necessary to rebuild the entire neutrino beam line, it is possible to influence all these aspects of beam production; they are also discussed in detail here. Finally, the civil construction relating to the beam systems is described.

III.1 Neutrino energy spectrum

The means by which the energy spectrum can be adjusted is illustrated with the density plot shown in Fig. 1. In this plot it can be seen how the spectrum is softened by increasing the distance of the detector from the axis defined by the center line of the decay tunnel. This is explicitly illustrated in Fig. 2 in which detector width slices of Fig. 1 are shown in one degree steps. The arrows along the abscissae mark the positions of the peaks, and show that the peak energies shift from about 1.3 GeV for the on-axis spectrum to 0.5 GeV for the spectrum 3 degrees off-axis. A further, dramatic illustration of the way in which moving off axis can shape the energy spectrum is shown in Fig. 3, in which the zero degree spectra are overlaid with the 1.5 degree off-axis spectra for detectors located 1, 3, 24, and 68 km from the source. The peaks are clearly shifted to lower energies in the off-axis cases, and in addition there is more flux at these important lower energies. Furthermore, the suppression of the high energy regions of the spectra is also desirable; there will then be lower probability for a high energy event to appear at lower energy. In any case, only those events whose initial energy is less than 4 GeV can be fully contained in the detector.

The reason why the neutrino spectra behave this way can be understood simply from the conservation of momentum and energy. For a pion decaying along a direction defined by the axis of the tunnel, the conservation laws lead to the neutrino energy given by

$$E_\nu = \frac{m_\pi^2 - m_\mu^2}{2(E_\pi - p_\pi cos\theta_\nu)} \tag{1}$$

where m_π and m_μ are the pion and muon rest masses,

E_π is the pion energy,

p_π is the pion momentum,

and θ_ν is the angle at which the neutrino is emitted.

Differentiating this expression shows that for a given neutrino emission angle, there is a maximum neutrino energy given by

$$(E_\nu)_{max} = \frac{m_\pi^2 - m_\mu^2}{2E_\pi^m sin^2\theta_\nu} \tag{2}$$

For pion energies both greater and less than E_π^m, E_ν is less than $(E_\nu)_{max}$. A plot of Equation 1 for neutrino detection angles of 0.0, 1.5 and 3.0 degrees is shown in Fig. 4 to illustrate this point. The curves show that at zero degrees, the neutrino energy is proportional to the pion energy, but in an off-axis direction, there is a maximum in the neutrino energy.

This behavior can be qualitatively understood by considering the transformation from the isotropic decay of a pion in the center of mass to the Lorenz enhanced decay distribution for a pion moving in the laboratory. This is illustrated in Fig. 5 which shows a sequence of momentum distributions of neutrinos emitted from successively faster moving pions. Because there is a maximum neutrino momentum (29.8 MeV/c) perpendicular to the pion's momentum, there is a maximum neutrino momentum at any given angle from the pion direction. Further, this maximum momentum is lowered as the observation angle is increased, as evident from Fig. 5 and shown explicitly in Fig. 2.

From Fig. 4 for the 1.5 degree off-axis case, pions with energies between about 2 and 7 GeV yield a neutrino energy near 1.0 GeV. Typical trajectories of pions that pass through and are focussed by the magnetic horns are plotted in Fig. 6. For pions between 2 and 7 GeV the focusing is essentially point-to-parallel, and it can be expected that the neutrino energy spectrum will peak near 1.0 GeV, as in Fig. 3. The fact that a wide range of pion energies map essentially to a single neutrino energy also explains the increase in flux at this lower energy relative to the on-axis beam.

Further illustration of neutrino beam behavior can be found from projections of the various energy bins of Fig. 1 onto the direction transverse to the central beam axis (the ordinate of Fig. 1). Several of these plots are shown in Fig. 7. Note that as the energy increases, the neutrinos go forward into progressively narrower cones. This behavior is predicted by Equation 2; neutrinos of energy larger than $(E_\nu)_{max}$ must lie in a forward cone defined by an angle smaller than θ_ν. This observation helps to clarify why a detector located on the central axis has such a large high energy tail. It is apparent that by shifting the position of the detector, the flux of neutrinos in any given energy interval can be maximized, thus

determining the optimum off-axis position at which to place the detectors.

The calculated transverse spreads of the neutrino beam at the distances of the various detectors are shown in Fig. 8. The fall-off with off-axis location shows there will be variation in intensity across the face of each detector. This point is illustrated in Fig. 9. For D1, the intensity varies linearly by $\pm$ 25 % relative to the midlife, and for the two far detectors the distributions are essentially flat across the detectors. Fig. 10 shows how the neutrino spectrum shape changes for a 14m by 14m fiducial size located at several distances from the neutrino source. The scale for each plot has been corrected by the $1/r^2$ behavior expected for a point source. The spectrum change from D1 to the far detectors is clearly not significant; furthermore, a simple linear fall in intensity across the face of the detectors does not change the $1/r^2$ dependence of the count rates in the detectors. Consequently, off-axis placement of the detectors will not cause significant systematic errors in the estimates of the fluxes expected in the far detectors. See Chapter V for details.

The way in which the neutrino energy spectrum can be tuned to match the goals of the experiment is clear. The detectors will be placed 1.5 degrees off-axis; it can be seen in Fig. 2 that although the peak energy is lower at 3 degrees, the flux is beginning to decrease significantly. Again, this can be understood by reference to Fig. 4 which shows that while the maximum neutrino energy is lower at 3 degrees, a smaller range of pion energies map to this maximum energy.

A more explicit way to determine the optimum angle is through the figure of merit (FOM) referred to in Chapter II.

$$FOM = \sum_{E_\nu} \phi(E_\nu)\sigma(E_\nu)/E_\nu^2 \tag{3}$$

where $\phi(E_\nu)$ is the flux as a function of neutrino energy E_ν,
and $\sigma(E_\nu)$ is the cross section.

This figure of merit is plotted in Fig. 11, which shows less than 10% variation from about 0.75 degrees to 2 degrees. Consequently, other factors, such as ease of placement, can be considered when choosing the exact location of the detectors.

Other methods of shaping the neutrino spectrum have also been investigated. The most straightforward is to use momentum selection devices in the horn, but it is already known from previous experience at the AGS [2] that there would be an accompanying unacceptable reduction in intensity.

It might naively be expected that lowering the proton beam energy would reduce the high energy tail. A plot of the spectra expected in D24 for both the on-axis and 1.5° off-axis cases, for proton energies of 12 GeV and 28 GeV, is shown in Fig. 12. The on-axis spectrum at 12 GeV indeed has a somewhat lower high energy tail than the 28 GeV spectrum, but the effect is not nearly as dramatic as is the effect of moving off the axis. The main result of lowering the proton energy is simply to reduce the overall flux of neutrinos, at low energies as well as high energies.

The simulation spectra above have all been generated assuming a proton beam that strikes the target on center and parallel to the target axis. Furthermore, the integrity of the target has been assumed, which will be discussed in section III.3.3. Simulation studies have been made to investigate the effects expected if these conditions are not met. An example of a case in which the detectors are at the same offset angle but 180° apart in azimuth is shown in Fig. 13. The proton beam has been mis-steered so as to strike the target 1.6mm (half the target radius) off-center. There would be a significant spectrum difference between the left and right detectors in this case, so that the prediction of the neutrino flux at a detector on one side of the beam axis from observations in a detector on the other side of the axis would be uncertain without calculated corrections. It will be seen in Chapter V that the actual separation of the far detectors, D24 and D68, is 10^0 in azimuth, so the effect in Fig. 13 is unimportant. A second example is shown in Fig. 14 in which the proton beam is directed onto the target at a small angle (7mrad), chosen so that the beam remains within the endcap of the decay tunnel. Again a small spectrum shift is evident. The AGS proton beam is routinely kept and monitored within 1 mrad.

III.2 Neutrino beam intensity

There are a variety of ways by which the intensity can be increased over that of the previous beam at the AGS. A straightforward improvement, nearly independent of neutrino production considerations, has already been achieved with the recent addition of the Booster ring. The proton beam intensity has been raised to over 5×10^{13} protons per pulse, and the goal of 6×10^{13} is within reach, to be compared with the previous maximum of 2×10^{13}. However, this higher current might introduce new problems not encountered in the earlier AGS experiments. These are dealt with in section III.3.3.

Other straightforward ways to increase the intensity are to lengthen and/or widen the decay tunnel. The previous tunnel was 52m long; Fig. 15 indicates that lengthening it to

240m would result in about a factor of three increase in flux. The old tunnel was 1.84m in radius, but from Fig. 16 there is not much gain (about 13%) if it were widened to 3m radius. It is also seen from Fig. 16 that for a tunnel 3m in radius half the flux comes from the innermost 60cm. It is too expensive to consider a tunnel more than 2m in radius; again, 90% of the flux for a 2m radius tunnel originates in the innermost 1.5m. We have used a radius of 1.5m and a length of 180m for our simulations; the actual design of the tunnel in Section III.3.4 calls for a tunnel with a aperture that varies with distance.

The use of a horn as the first element in the pion focusing system has also been scrutinized. Possible alternatives, such as a large aperture Li lens of the type used extensively at the CERN and Fermilab antiproton production sources, or a plasma lens such as the one under development at Erlangen [3], might be a superior option. Shown in Fig. 17 is a comparison of simulation studies of a system using a z-pinch plasma lens as the first element with one using a horn [4]. The parameters used in this calculation were precisely those of the former Brookhaven neutrino line [5]. At most, 75% of the horn focused flux can be obtained with this lens. Another problem, common to both plasma and lithium lenses, is that it is difficult to build such devices with an aperture large enough for an intense neutrino beam. In the case of antiproton production the source is very bright and tightly focussed, but this is not the situation here. Therefore, our beam design has been based upon a double horn system. An important consideration, besides the difficulties with other devices mentioned above, is that horns are a well-known and well-tested technology.

III.3 Detailed description of the neutrino beam

The fast extraction of the proton beam for E889 from the AGS is basically the same as for RHIC and the g-2(E821) experiment. It is done with the same kicker magnet at the same location. However, the duration of the kicker pulse for E889 will be sufficient to extract all of the beam in the AGS ring. The micro-structure will consist of 8 rf buckets. The extracted protons are transported to the 'U' line where the new proton transport for E889 branches off. The facilities for production of the new neutrino beam can be functionally separated into five regions as shown in Fig. 18.

- A conjunction area where the proton transport for E889 splits off from the present 'U' line proton transport in a bend of 12°, and is optically matched into the large bend to the neutrino target.

- The proton transport section where the protons are bent further to a total of 60.5° to aim the neutrino beam in the desired direction. Also included are the final focusing and correcting trims.

- The horn/target area in which pions are produced by the interactions of the proton beam with a target inside the first focusing horn. The second horn creates a parallel beam of pions directed toward the end of the decay tunnel. This area is the maximum radiological concern since the entire AGS beam is striking the target and creating a high level of activation and possible radiation damage.

- The decay tunnel is a simple shielded tunnel, probably filled with helium for most of its length. The length (180m) and diameter (3m) are sufficient to allow most of the pions to decay.

- At the end of the decay tunnel is a massive block of steel shielding to absorb the protons and undecayed pions to avoid activating the soil. In this absorbing block there are a series of slots which allow the muon distribution to be sampled.

Details of the beam production components in these regions are discussed in the following subsections. Civil construction is discussed in section III.4.

III.3.1 Conjunction area

In terms of beam components, the conjunction area is relatively simple. There are 5 dipoles and 4 quadrupoles to bend the beam by 12° and match the beam size into the large bend. Since this section is connected to the existing RHIC transport line, there are a number of constraints in space and time which must be met. Discussions have been held with the RHIC accelerator staff which indicate that these constraints can be met. No RHIC beam line elements need to be repositioned, and there are a number of possible time windows which will allow the necessary civil construction of this conjunction tunnel to be carried out. A conceptual design for radiation safety for all the affected lines has been considered.

III.3.2 Proton transport section

The large bend in this portion of the transport is accomplished with the use of RHIC injection line (room temperature) gradient dipoles of the 'C' type with a 3.8cm vertical gap. Existing designs and tooling make the construction of these 20 dipoles relatively quick and

straightforward. Calculations show that the vertical aperture in these dipoles is nearly twice that required for the 100π mm mrad emittance of the fast extracted proton beam from the AGS. Trim magnets are included between each dipole to keep the beam well centered in the gradient dipoles.

In the final section a set of 4 quadrupoles focuses the beam on the pion production target in the horn. Vertical and horizontal trim magnets provide for steering the beam onto the target.

To keep the proton beam accurately centered on target, a number of instruments are provided along the proton transport. In the dipole arc there are loss monitors, plunging scintillation flags and EPM's (residual gas profile monitors). Just before the target there is a current transformer to measure the intensity, and a series of SWICs to measure the beam position. Beam position monitors developed at TRIUMF for KAON might be preferable to the SWICs in that they are nonintercepting and do not disturb the beam. In either case, it will be possible to maintain the beam position on the target to within 0.1mm of center and the angle of incidence to within 0.5mrad.

The interacting flux is measured with ionization chambers at 90° to the target. Beam timing will be determined by lucite Cherenkov counters.

III.3.3 Horn/target area

The present pion focusing system is based on two horn focusing elements as shown in Fig. 19. The large magnetic fields (up to 5T) created by the high currents (up to 250 kA) in the first coaxial horn provide strong focusing on the produced particles contained in the narrow neck of the first horn. For a broad range of momenta above and below 3 GeV/c, there is an intermediate focus between the two lenses. The second horn takes the beam from point to parallel down the decay tunnel. Water cooling is necessary in the first horn since there is heating from both the current on the inner conductor and heat deposition in the target. Calculations are being done to check whether the previously used cooling capacity [6] will be adequate in view of the increased proton current.

As noted in section III.2 there may be some new technical difficulties encountered because of the increased proton beam current. These include an increase in the average beam power deposited in the production target and focusing devices, a larger density of energy deposition in the target, increased air activation and ionization in the target region, and the necessity for remote handling of the target and focusing elements. All have been dealt with at other

laboratories and should not present a serious challenge or require new technology to solve.

Too high an energy deposition in the target could cause melting in the central region [7], which would result in a loss of density of the target material. An example of this effect is shown in Fig. 20. The calculation was done for a copper target 50cm long and 7mm in diameter, and the beam was contained in a 3mm (4σ) diameter spot. There were 10^{13} protons per pulse, fewer than anticipated in this experiment, and the pulses were 1.5s apart in time. The plot shows the variation in target density along the rod for the first few pulses, and it is seen that at the downstream end of the rod the density is barely 60% of the initial density after only five pulses.

A serious problem can arise if the energy deposited by the beam is restricted to too small an area of the target[7]. In this case, shock wave propagation can result in destruction of the target. These problems have been solved for antiproton production targets at a number of laboratories. It has been found that a combination of adequate cooling, target containment, and sufficiently spread out proton beam result in a target that lasts for long periods of time [8]. Doubling the diameter of the beam will result in the same energy density deposition in the target as in the previous AGS beam. The diameter of the target would then have to be doubled to accommodate the larger beam. This would result in a 10% reduction in the neutrino flux, as shown in Fig. 21. Detailed calculations are underway for a target design that will withstand all these effects.

Increased proton current will introduce new difficulties in the horn system. The water cooling arrangement for the target and horn system inherently requires that these systems be operated in air (or some other atmospheric environment). AGS safety personnel indicate that activation of the air should not pose a serious problem provided the target area and decay tunnel are sealed and the enclosed atmosphere controlled and monitored. The effects of ionization of the air in the vicinity of the high voltage pulsed focusing devices were not a problem at 2×10^{13} protons per pulse, but need to be investigated for the higher intensities anticipated here. However, since the area must be sealed and the atmosphere controlled, such problems could be solved by a suitable choice of gas mixture or improved insulator design, and these options are being investigated.

Remote handling of the target and horn systems may possibly be required and with the increased current may need to be more elaborate than before. TRIUMF, LAMPF, PSI and the antiproton production sources at CERN and Fermilab provide adequate examples of how to resolve the anticipated remote handling problems. It is planned to hang the horns in narrow shielded caves as shown in Fig 14. This is a technique used at the AGS as well as

other laboratories. This problem can be resolved through attention to design details. It may be necessary to provide a rudimentary hot cell and manipulator facility close to the target area.

It will be necessary to build a new supply to power the horns. The high current required, approximately 250 kA, is produced by the discharge of capacitor banks through the horn inductances. The switch in the supply used previously was a series of ignitrons. A pulser using SCRs as the switch has recently been designed at TRIUMF. It is based on the proposed CERN LHC abort kicker system. The SCR design is a new technology for pulsers of this type, but would have several advantages over the ignitron design, such as reduced jitter and improved lifetime. On the other hand, ignitrons have the advantage that they have been operated successfully and are a well known technology at BNL. It is planned to prototype both types of system, and choose between them largely on the basis of reliability.

It might prove advantageous to power each horn with a separate supply; the pulse duration can then be shorter and the ohmic heating effects would be reduced. Calculations are underway to determine whether the modest extra expense would be justified. The supply will be capable of delivering 250kA to the horns but it will run routinely at 200kA, because the undesirable heating and mechanical shock effects vary quadratically with voltage and current. It is shown in Fig. 22 that, although the neutrino yield peaks near 250kA, there is only a 5% loss in running at the lower current.

III.3.4 Decay tunnel

The decay tunnel consists simply of round pipe sections, and will be 180m long as noted in section III.3. The upstream half will be 2.4m in diameter and the downstream portion will be expanded to 3m. It is planned to fill the tunnel with helium since this reduces the 20% interaction probability by a factor of 5. Since this space is unoccupied by persons or equipment, no facilities are required in the decay tunnel.

III.3.5 Beam stop

The beam stop will be a cube of steel, about 6m on a side. This probably will be assembled from blocks made out of recycled steel from Oak Ridge. The stop serves two purposes. First it is long enough to attenuate all the strongly interacting particles in the beam to a level where soil activation is no longer an issue. Second, by placing slots at various depths in the steel, the angular distribution of muons for various energies can be measured with arrays of

small ion chambers, as was done during E734 [5]. Since the muons result from the same pion decays which produce the neutrinos, the muons are a good monitor of neutrino beam and a measure of their energy spectrum.

III.4 Civil construction

In this section the civil construction for the proton transport, target/horn building, and decay tunnel is discussed.

A plan view of the new facilities for producing the neutrinos for E889 is shown in Fig. 23. Represented in this figure are the proton transport tunnel, pion decay tunnel, beam dump, target/horn building, the earthen shield, and the existing structures near the fast extracted beamline.

Several existing utilities require modification for the construction of the new beamline. Catch basins and storm drains used for surface drainage will require relocation. An existing water pipe will be replaced to withstand the increased pressure caused by the earthen shield. Some small storage sheds in the area need to be relocated or demolished. One of the more expensive modifications will be the re-routing of Thomson Road around the beam dump. The schedule of these modifications will be carefully coordinated with the beamline construction.

Three buildings will be built for the beamline. Early completion of the horn/target building is essential for construction and testing the new horn system. The building will be of similar construction to the slow beam experimental halls. The building has been sized (5000 ft^2) to house the proton target and pion focusing horns, the horn power supply systems, power supplies for magnets in the later portion of the proton transport, and the closed loop water cooling system for the horns. A 25 ton crane will be used for shielding and horn rigging operations. A shielded storage area will house an activated horn should it require removal after operations. The shielding around the target area will occupy a large portion of the building. Besides the usual building utilities, substantial electrical power will be distributed to specified locations for the horn and magnet power supplies. The target/horn building construction and utilities will be completed within six months after the start of construction.

The remaining two structures can be completed at a later time in the construction schedule. A 900 ft^2 power supply building will be located near the beginning of the proton transport. It will house the power supplies for the initial portion of the new proton beamline. A small roofed structure will be built over a portion of the beam dump which has muon detectors. This structure will serve as a weather shield for the detectors which will be placed

into slots inside the iron dump.

The construction of the conjunction area where the proton transport is joined to the existing U-line will be coordinated with AGS operations. During the 3 months required for the construction of the conjunction area, there can be no beam extracted from the AGS into the U-line. The area will be excavated and a portion of the existing tunnel will be enlarged to accommodate the first bending dipoles. Shielding will be placed along the existing tunnel. This should enable a portion of the proton transport tunnel to be occupied in the future while beam is delivered to the g-2 target station or RHIC. Finally, the front portion of the proton transport tunnel will be installed and sufficient earthen shielding replaced before it will be permitted to extract any beam into the U-line.

The proton transport and decay tunnels are similar to previous tunnels built for the AGS Booster and RHIC transfer line. A plan view of the tunnels is shown in Fig. 18. The proton transport tunnel will be built of 11 foot diameter corrugated pipe sections. A concrete slab will be poured for a tunnel floor. There will be an emergency escape hatch near the beginning of the tunnel. The main entrance has been sized for installation of the magnets and is located near the target building. The completed tunnel will have lighting, ventilation, fire detection/protection, emergency lighting, and power distribution. The earthen shielding on top of the tunnel will be 20 feet thick and considerably thicker on the sides. This thickness is required to reduce potential radiation levels outside the tunnel both from normal beam losses and from fault conditions. The decay tunnel will have a similar earthen shield.

Summary of Section III A.

The design and characteristics of the proposed new AGS neutrino beam are described. We have discussed at length the neutrino beam energy spectrum and spatial shape, and the evidence that offsetting the E889 detectors with respect to the proton beam center line has several important advantages for a long baseline neutrino oscillation search, and essentially no serious disadvantage. The variation of flux across the cross section of the detectors was shown; its explicit effect on the search for oscillations is treated in Chapter V. The detailed description of the several elements of the proton, meson, and neutrino beam was given, and the civil construction required for these elements specified.

References

[1] R. L. Helmer, in *Proc. of the 9^{th} Lake Louise Winter Institute*, Lake Louise, Canada, 1994, to be published, and TRIUMF preprint TRI-PP-94-34, June, 1994.

[2] A. Carroll et al., IEEE Transaction in Nuclear Science, **NS-32** (1985) 3054.

[3] J. Christiansen et al., in *Proc. of the European Particle Accelerator Conference* (EPAC90), Nice (1990), CERN/PS 90-30 (AR), p. 343 (1990).

[4] R. Weib et al., Universität Münster, Institut Für Kernphysik, Annual Report, (1992/93) p. 45.

[5] L. A. Ahrens et al., Phys. Rev. **D34** (1986) 75.

[6] W. Leonhardt et al., in *Proc. of the Particle Accelerator Conference*, Washington, D.C., (1987) vol. 3, p. 1740.

[7] T. A. Vsevolozhskaya, Preprint 84-88, Novosibirsk, 1984, unpublished. G. Silvestrov, in *Proc. of the XIII Int. Conf. on High Energy Accelerators*, Novosibirsk, 1986.

[8] T. Eaton, TRIUMF Design Note TRI-DN-89-K41, (1989), unpublished.

Figure Captions

Fig. 1. Density plot showing the variation in neutrino spectrum shape over a $\pm 3^\circ$ angular range 1.5km from the production target.

Fig. 2. Variation of neutrino spectrum shape for D1 located at several angles from the central axis. The arrows mark the positions of the peaks.

Fig. 3. Comparison of spectra for D1, D3, D24 and D68 located on axis (0°) and 1.5° off axis.

Fig. 4. Variation of neutrino energy with pion energy when the neutrino is observed in the direction of the pion decay (0°), and at angles of 1.5° and 3.0° from this direction. The upper part outlines the kinematics.

Fig. 5. Neutrino momentum ellipses for various pion momenta directed along the abscissa. The number labeling each ellipse is the pion momentum in GeV/c. Note the expanded ordinate scale. For a given pion momentum, the neutrino momentum in any direction is the length of the vector from the origin to the boundary of the ellipse in that direction.

Fig. 6. Typical pion trajectories through the horns. Each pion originated at the front of the target and was emitted at an angle of 0.1 radian. The number labeling each trajectory is the pion energy in GeV.

Fig. 7. Changes of neutrino flux at D1 in several energy bins as the distance off-axis is varied.

Fig. 8. Transverse spread of the neutrino beam at the distances of the various detectors.

Fig. 9. Distribution of neutrinos incident on a flat square offset by 1.5^0 from the beam axis. The fall of neutrino intensity is well fit by a function $A_0 + A_1 x + A_2 x^2$ where x is the distance transverse to the beam axis from the center of the tank. The neutrino spectra for the inner 1/3 (-7.5 m to -2.5 m), the middle 1/3 (± 2.5 m), and the outer 1/3 (2.5 m to 7.5 m) are shown at the bottom. The approximately 10% shift in the average energy from one side of the fiducial volume to the other is not a problem when the spectrum is folded with

the path-length and the cross section as shown in Chapter V.

Fig. 10. Variation in spectrum shape at several distances from the source. The fiducial size at each distance was taken to be 14m by 14m, and the center of each detector was 1.5° off-axis. The spectra were normalized to one another by correcting for the $1/r^2$ fall-off expected for a point source.

Fig. 11. The figure of merit (FOM) for D24 located at various angles from the central axis.

Fig. 12. The neutrino beam shape produced by 12.4 GeV protons (ANL, ZGS), 60m from the neutrino source and on the beam center line compared with the beam shape at 1.5^0 off axis produced by 28.3 GeV protons at 1 km from the source.

Fig. 13. Comparison of spectra in D1 located on either side of the central axis when the incident proton beam is displaced by 1.6mm to the left of the target center.

Fig. 14. Comparison of spectra in D1 located on either side of the central axis when the incident proton beam strikes the center of the target at an angle of 7mrad.

Fig. 15. Running sum of the percentage of neutrinos detected in D24 that originate in each 20m long section of the decay tunnel. The total tunnel length was 240m and the radius was 3m.

Fig. 16. Running sum of the percentage of neutrinos detected in D24 that originate in each 20cm thick cylinder of the decay tunnel. The total tunnel radius was 3m, and the length was 240m.

Fig. 17. Comparison of the neutrino flux obtainable with various focusing element combinations (from [4]).

Fig. 18. The facilities required for the production of the new neutrino beam.

Fig. 19. The pion focusing horns.

Fig. 20. Reduction in density along the central 1mm diameter core of the target as it is bombarded by five successive pulses of the proton beam. There were 10^{13} protons in each 2.5μs long pulse, 1.5s between pulses, and the beam width (4σ) was 3.2mm. The target was a copper rod 50cm long and 7mm in diameter, and it was in vacuum and not cooled. The numbers label the successive pulses.

Fig. 21. Comparison of neutrino spectra predicted for D24 with the previous proton beam ($4\sigma = 3.2$mm) and production target (diameter=6.4mm) (solid line) and with these two parameters doubled. The statistical errors on the sums are about 1%.

Fig. 22. Variation of neutrino yield with horn current, as observed at D3. The spectra were integrated from 0 to 6 GeV.

Fig. 23. Details of the new beam production area.

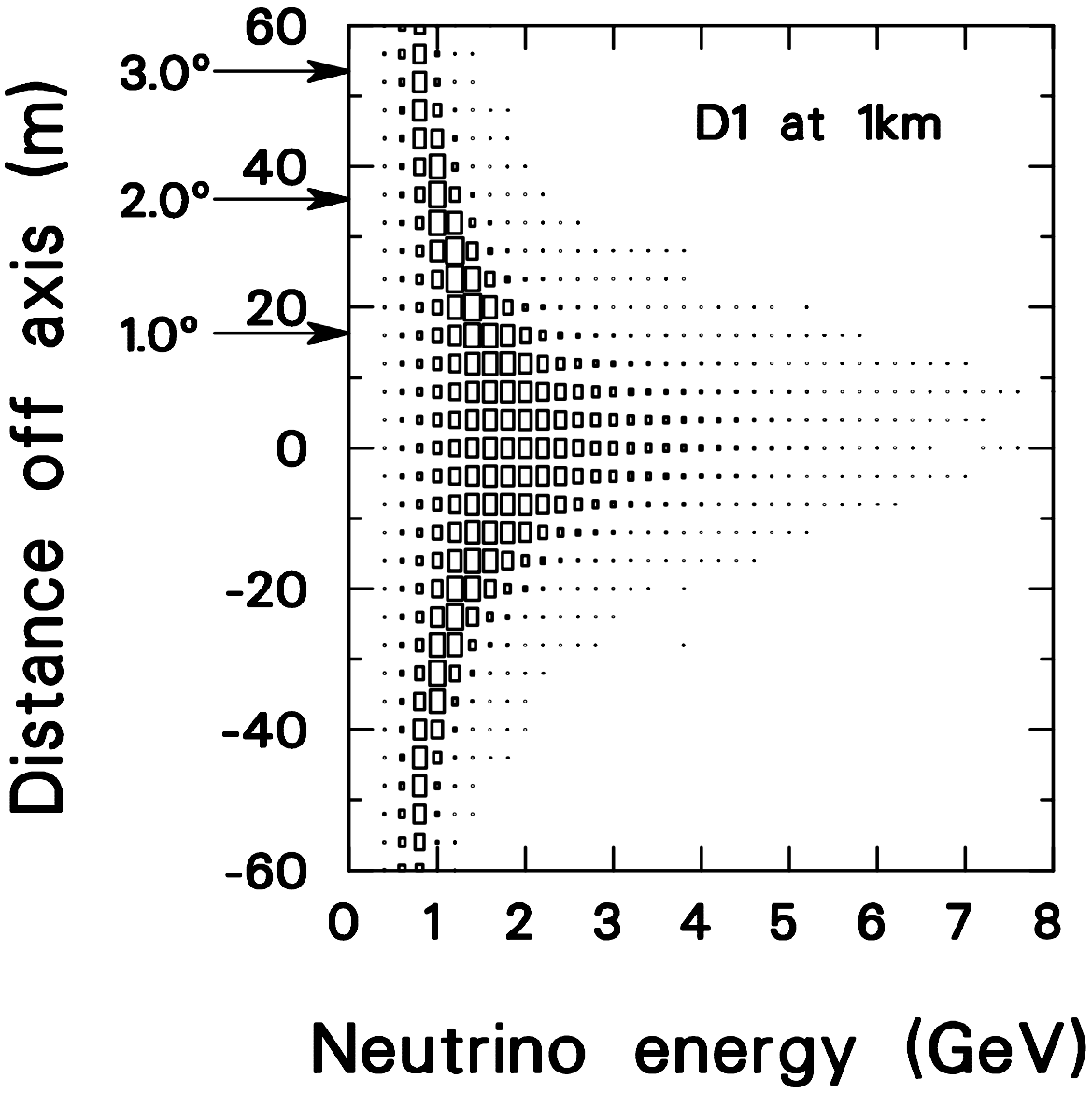
D1 at 1km
Distance off axis (m)
Neutrino energy (GeV)
60
40
20
0
-20
-40
-60
3.0°
2.0°
1.0°
0
1
2
3
4
5
6
7
8

Figure 1

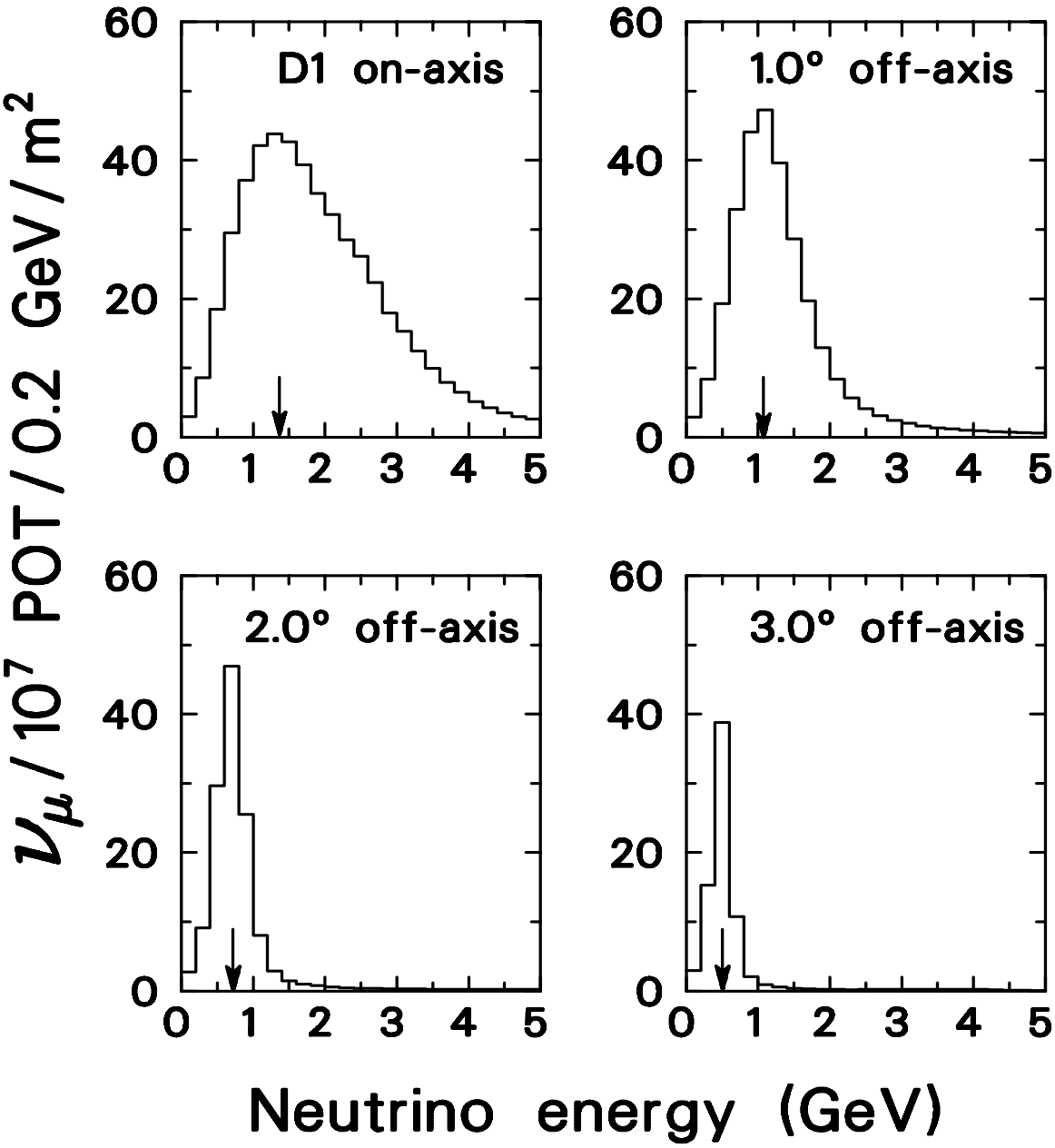
D1 on-axis
1.0° off-axis
2.0° off-axis
3.0° off-axis
ν_μ / 10^7 POT / 0.2 GeV / m^2
Neutrino energy (GeV)
0
20
40
60
0 1 2 3 4 5

Figure 2

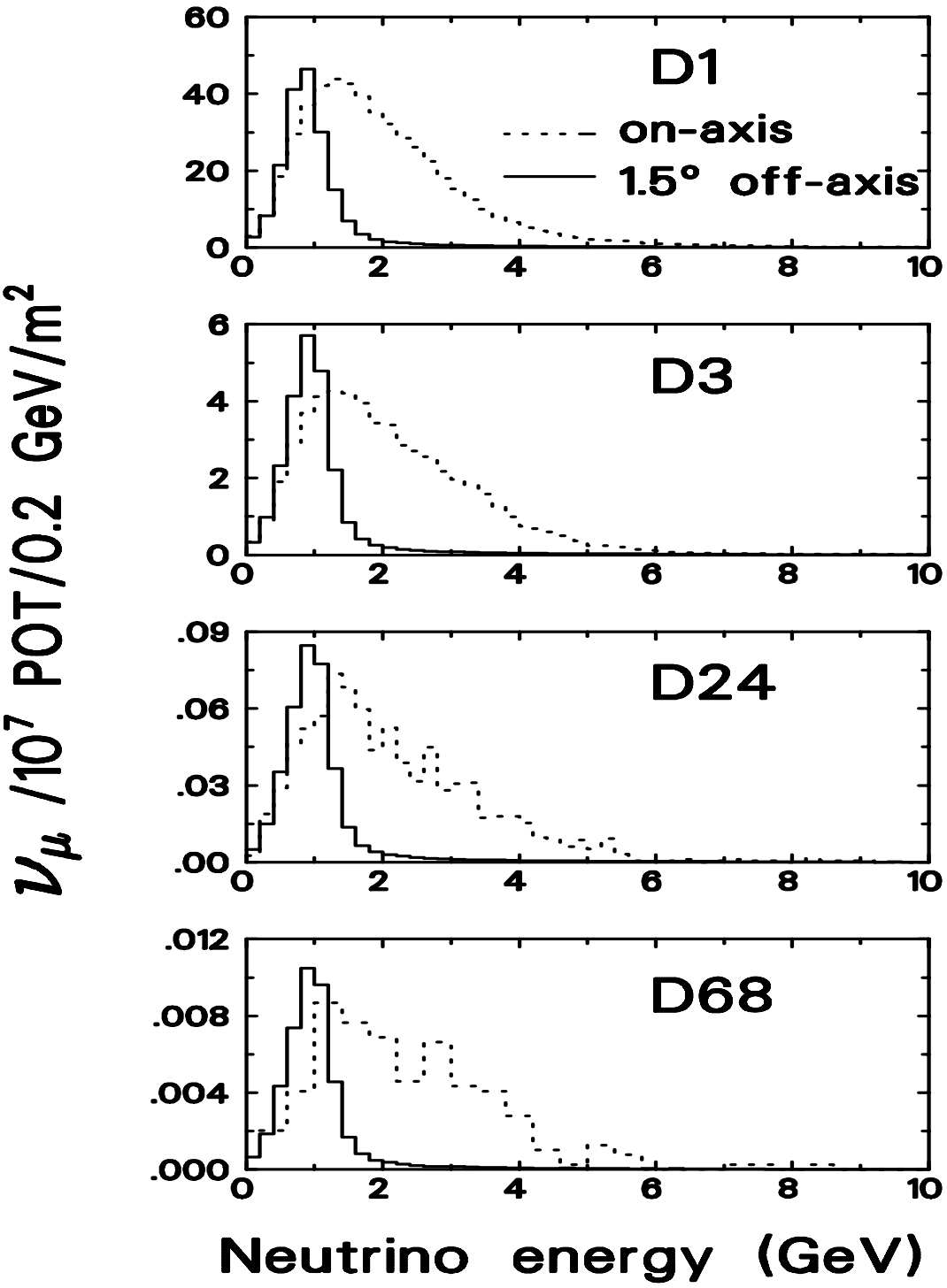
D1
on-axis
1.5° off-axis
D3
D24
D68
ν_μ /10^7 POT/0.2 GeV/m^2
Neutrino energy (GeV)

Figure 3

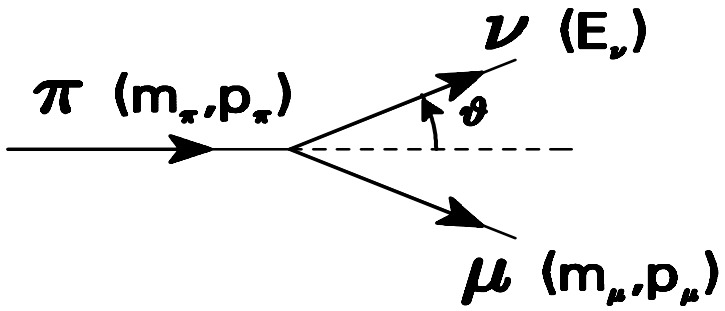

From energy, momentum conservation

$$E_\nu = \frac{m_\pi^2 - m_\mu^2}{2(E_\pi - p_\pi \cos\vartheta)}$$

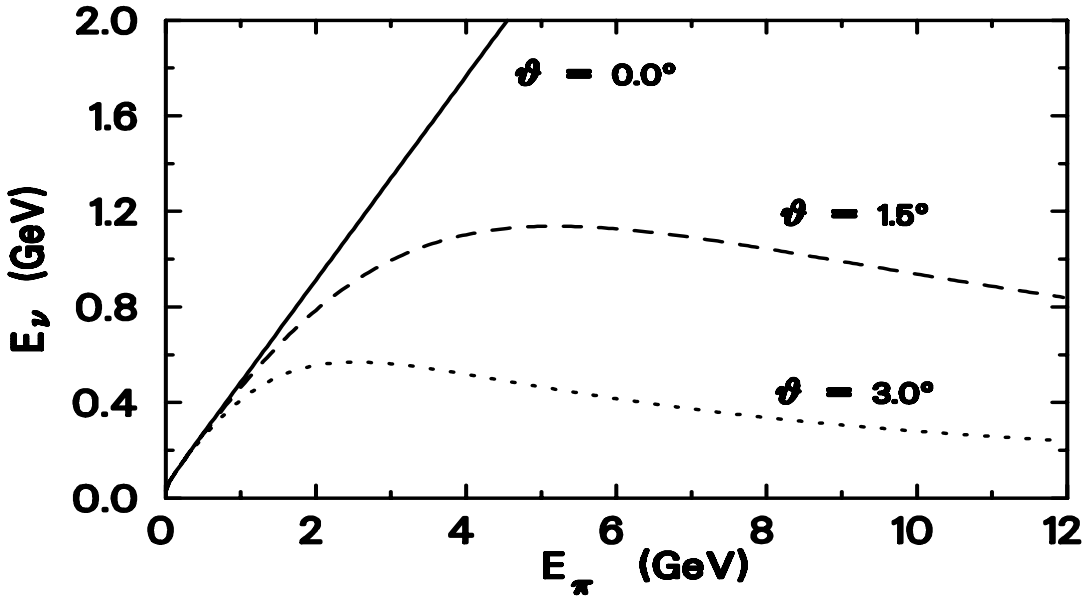

Figure 4

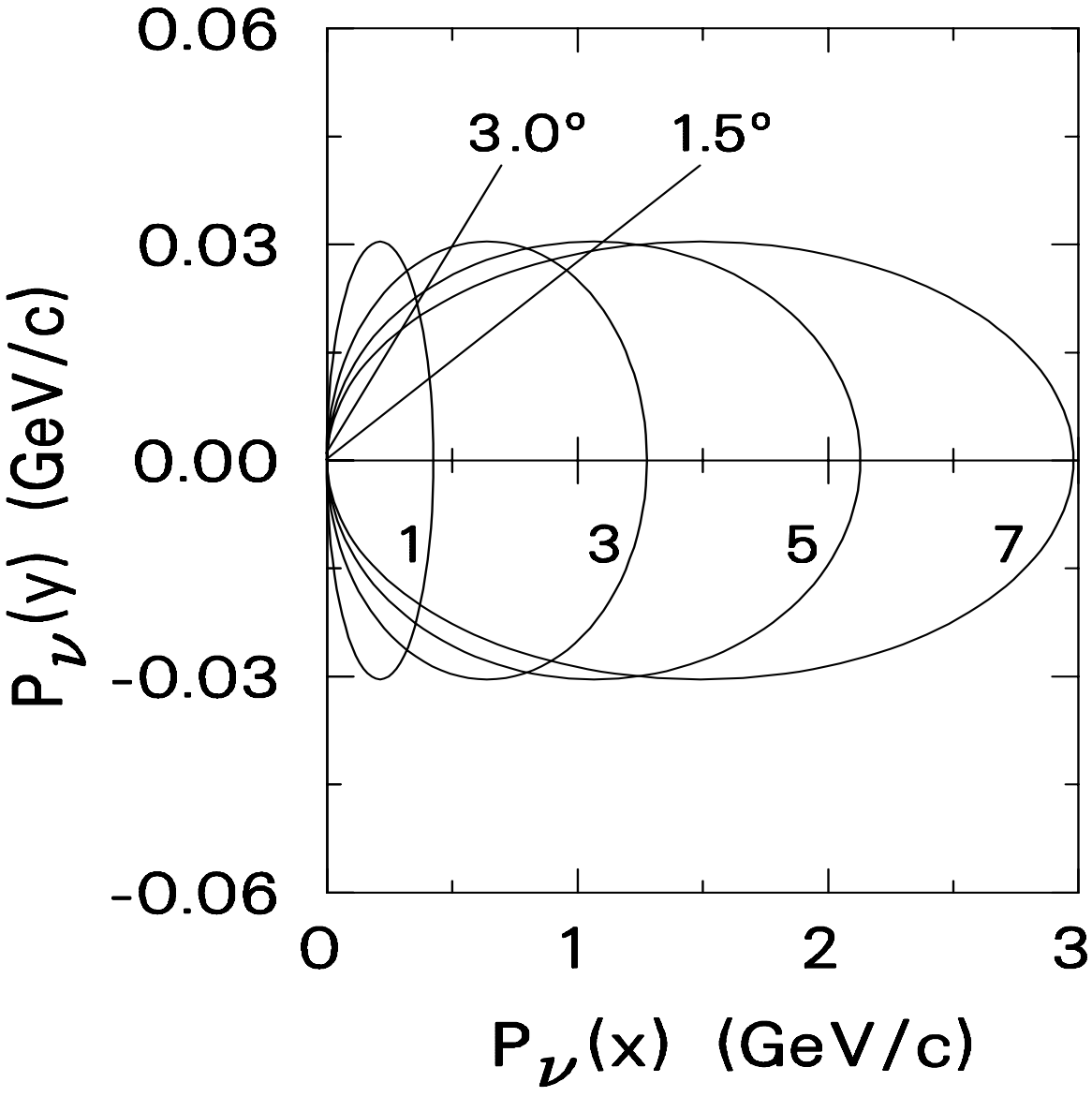

Figure 5

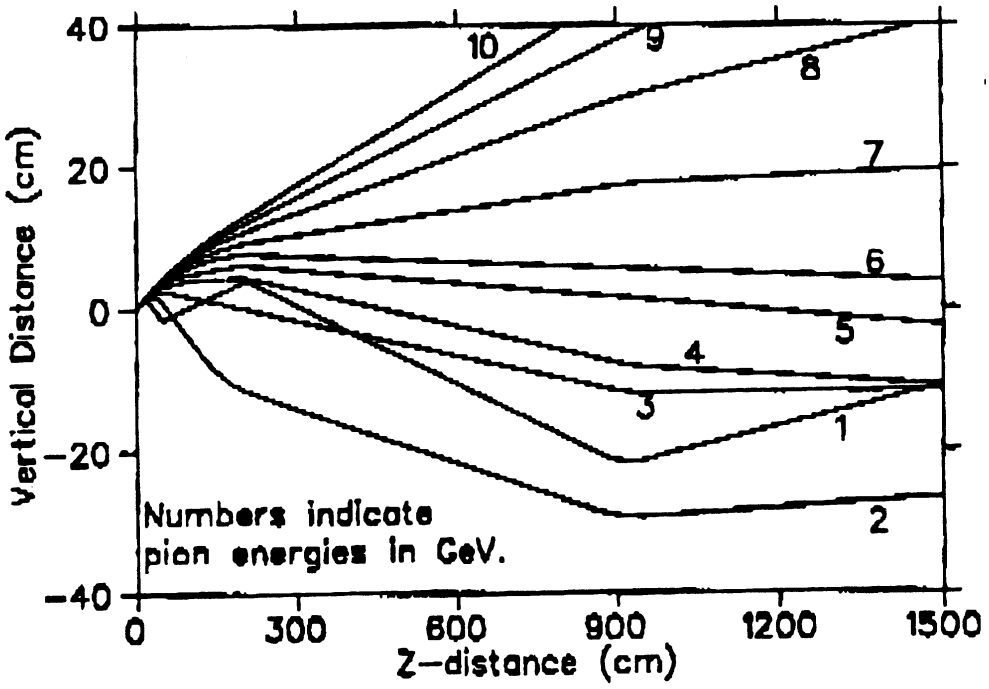
40
20
0
−20
−40
Vertical Distance (cm)
0
300
600
900
1200
1500
Z−distance (cm)
10
9
8
7
6
5
4
3
1
2
Numbers indicate
pion energies in GeV.

Figure 6

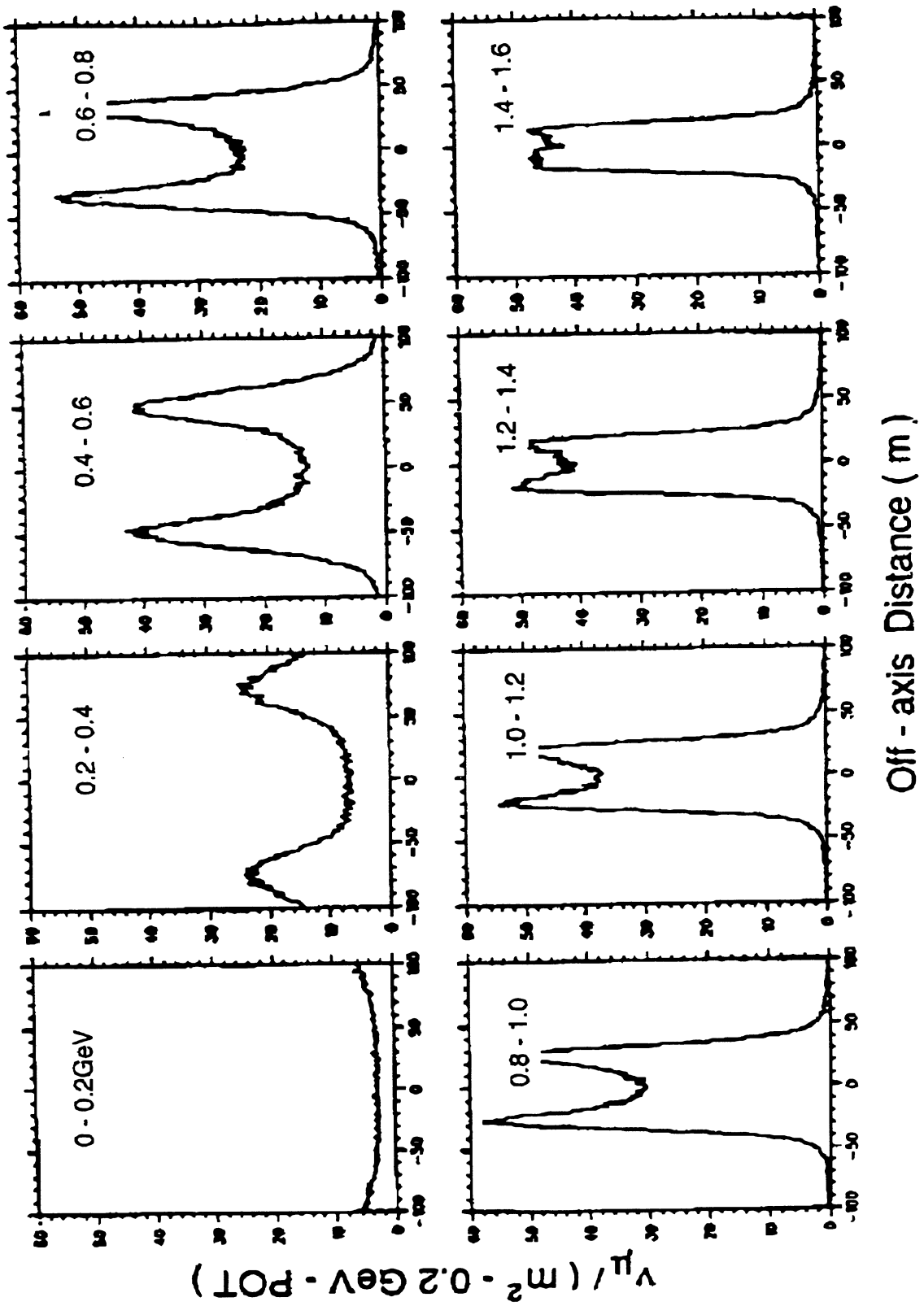
0 - 0.2GeV
0.2 - 0.4
0.4 - 0.6
0.6 - 0.8
0.8 - 1.0
1.0 - 1.2
1.2 - 1.4
1.4 - 1.6
ν_μ / (m^2 - 0.2 GeV - POT)
Off - axis Distance (m)

Figure 7

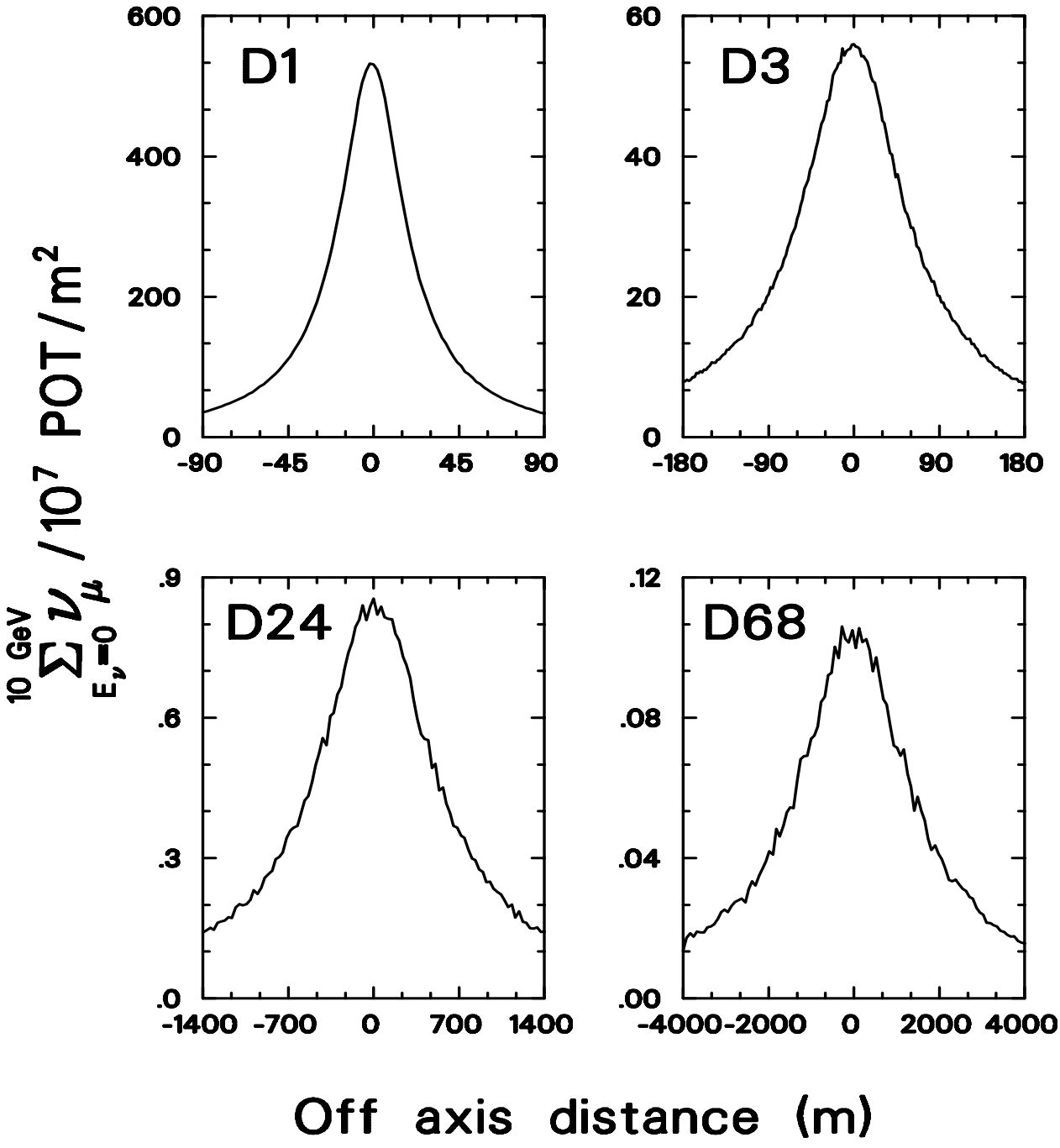
D1
D3
D24
D68
600
400
200
0
60
40
20
0
.9
.6
.3
.0
.12
.08
.04
.00
-90 -45 0 45 90
-180 -90 0 90 180
-1400 -700 0 700 1400
-4000 -2000 0 2000 4000
10 GeV
$\sum_{E_\nu=0} \nu_\mu$ / 10^7 POT / m^2
Off axis distance (m)

Figure 8

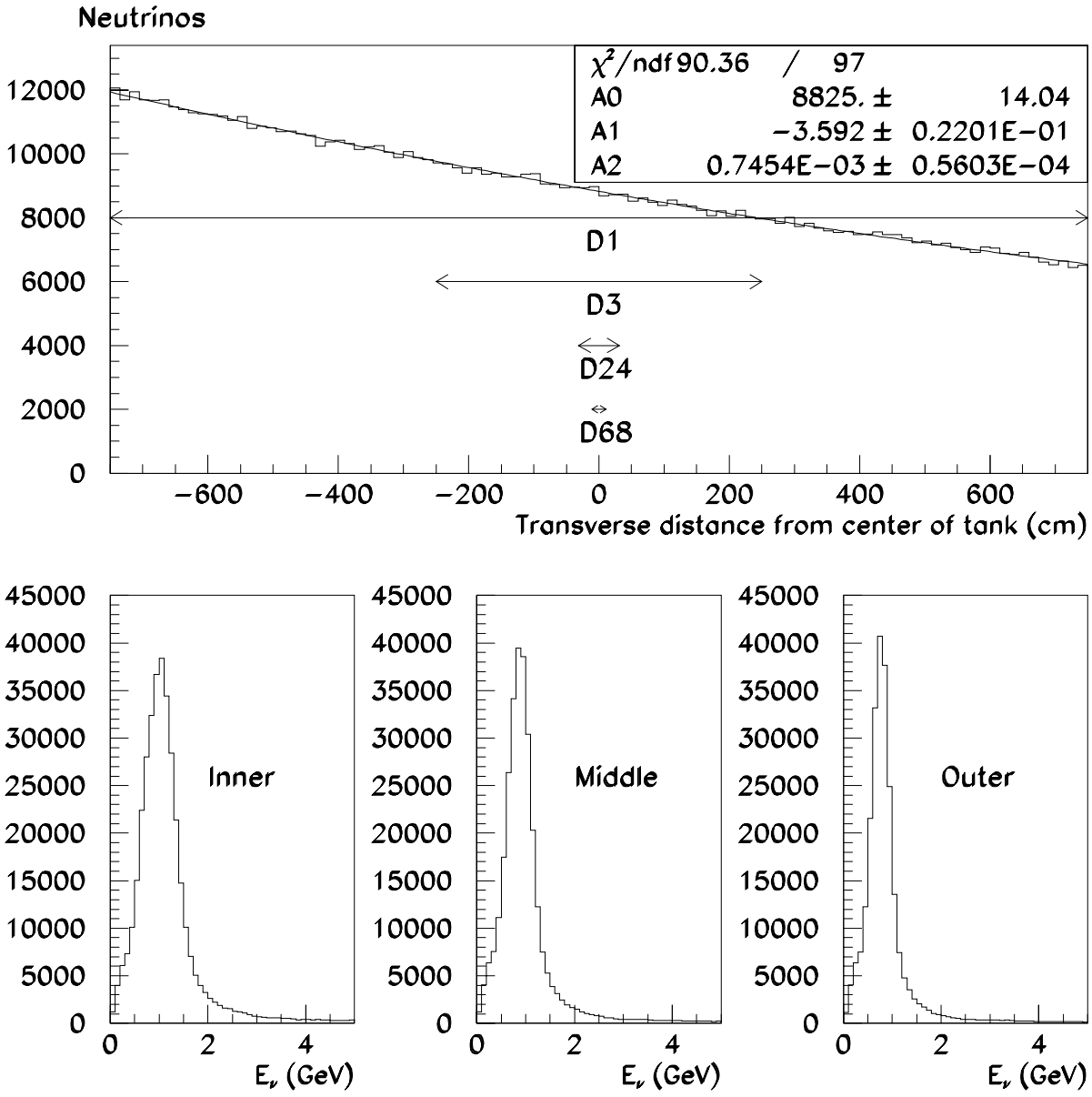
Neutrinos
χ²/ndf 90.36 / 97
A0 8825. ± 14.04
A1 −3.592 ± 0.2201E−01
A2 0.7454E−03 ± 0.5603E−04
D1
D3
D24
D68
Transverse distance from center of tank (cm)
Inner
Middle
Outer
E_ν (GeV)

Figure 9

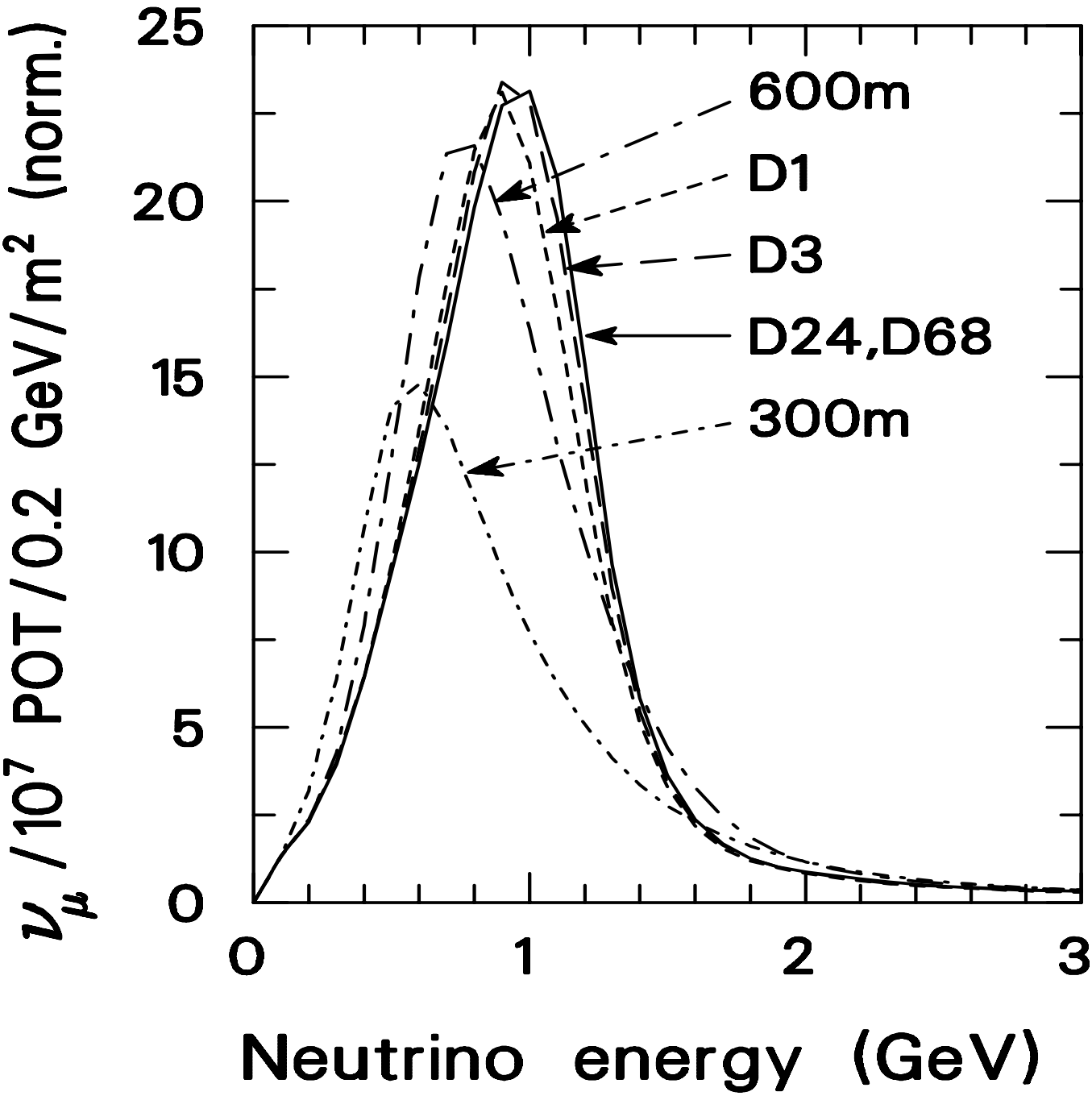
25
20
15
10
5
0
0
1
2
3
600m
D1
D3
D24,D68
300m
ν_μ /10^7 POT /0.2 GeV/m^2 (norm.)
Neutrino energy (GeV)

Figure 10

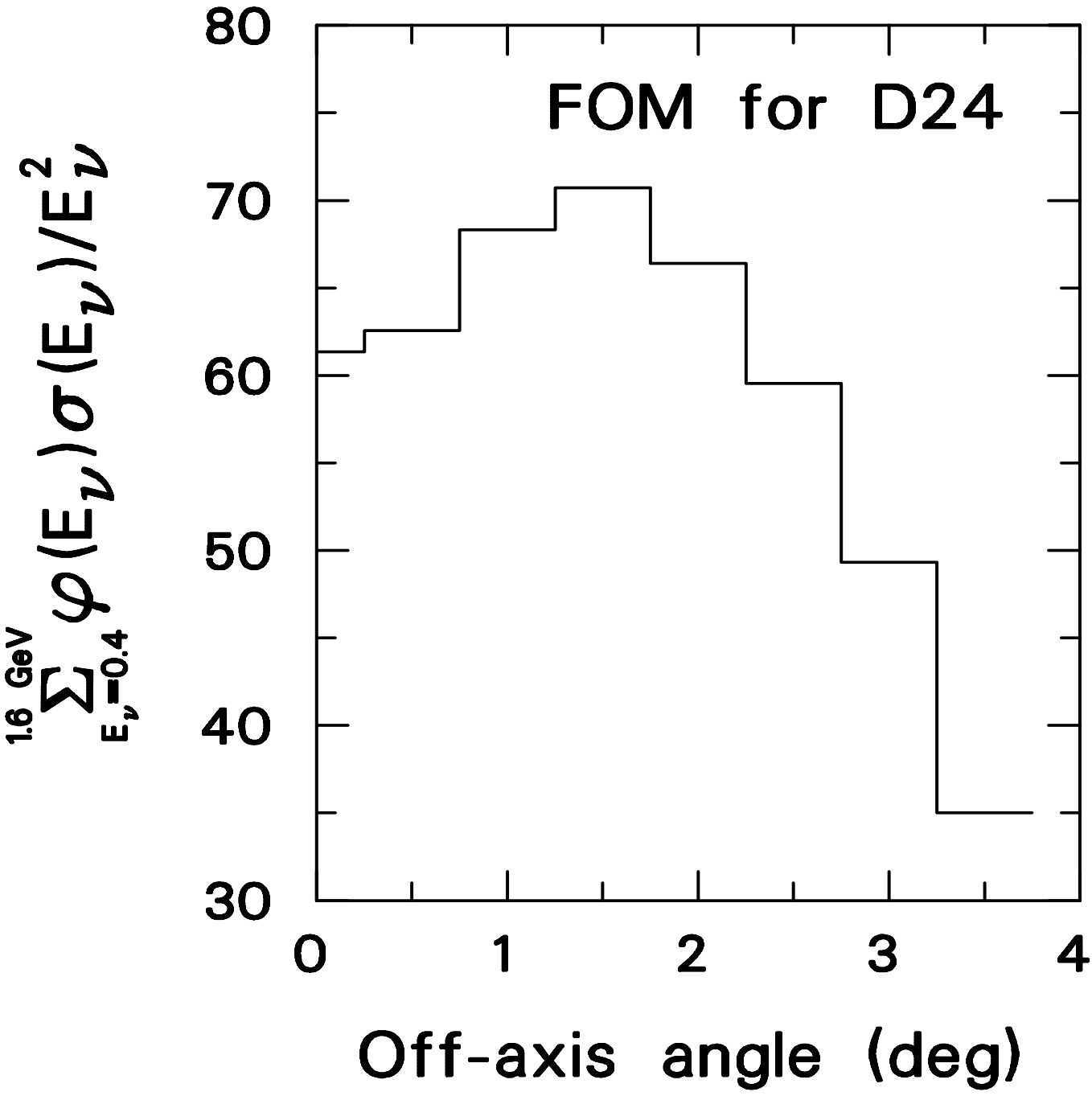
FOM for D24
80
70
60
50
40
30
0
1
2
3
4
Off-axis angle (deg)
$\sum_{E_\nu=0.4}^{1.6\ GeV} \varphi(E_\nu)\sigma(E_\nu)/E_\nu^2$

Figure 11

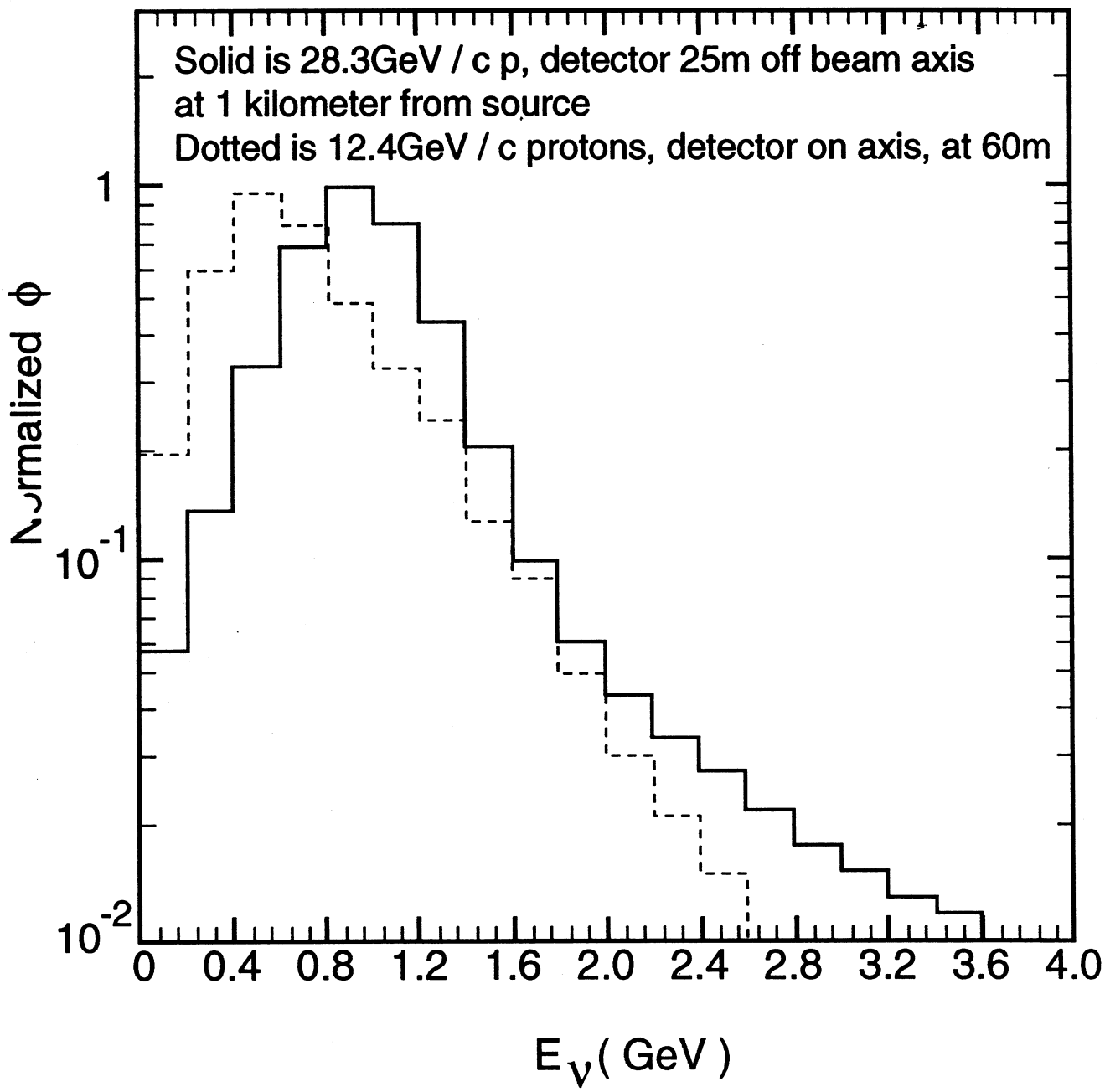
Solid is 28.3GeV / c p, detector 25m off beam axis
at 1 kilometer from source
Dotted is 12.4GeV / c protons, detector on axis, at 60m
Normalized ϕ
1
10^-1
10^-2
0
0.4
0.8
1.2
1.6
2.0
2.4
2.8
3.2
3.6
4.0
E_ν (GeV)

Figure 12

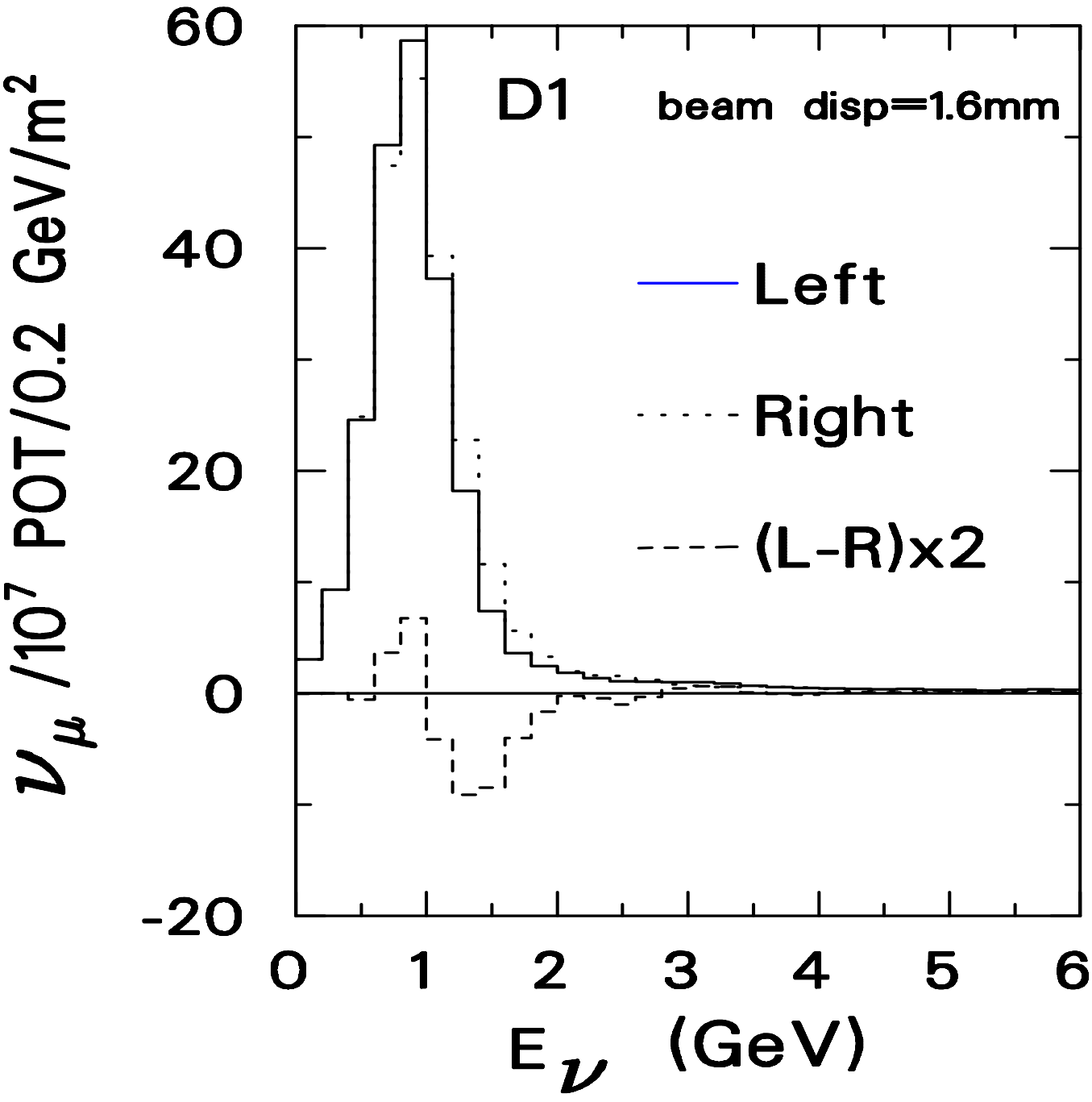
D1
beam disp=1.6mm
Left
Right
(L-R)x2
ν_μ /10^7 POT/0.2 GeV/m^2
E_ν (GeV)
60
40
20
0
-20
0
1
2
3
4
5
6

Figure 13

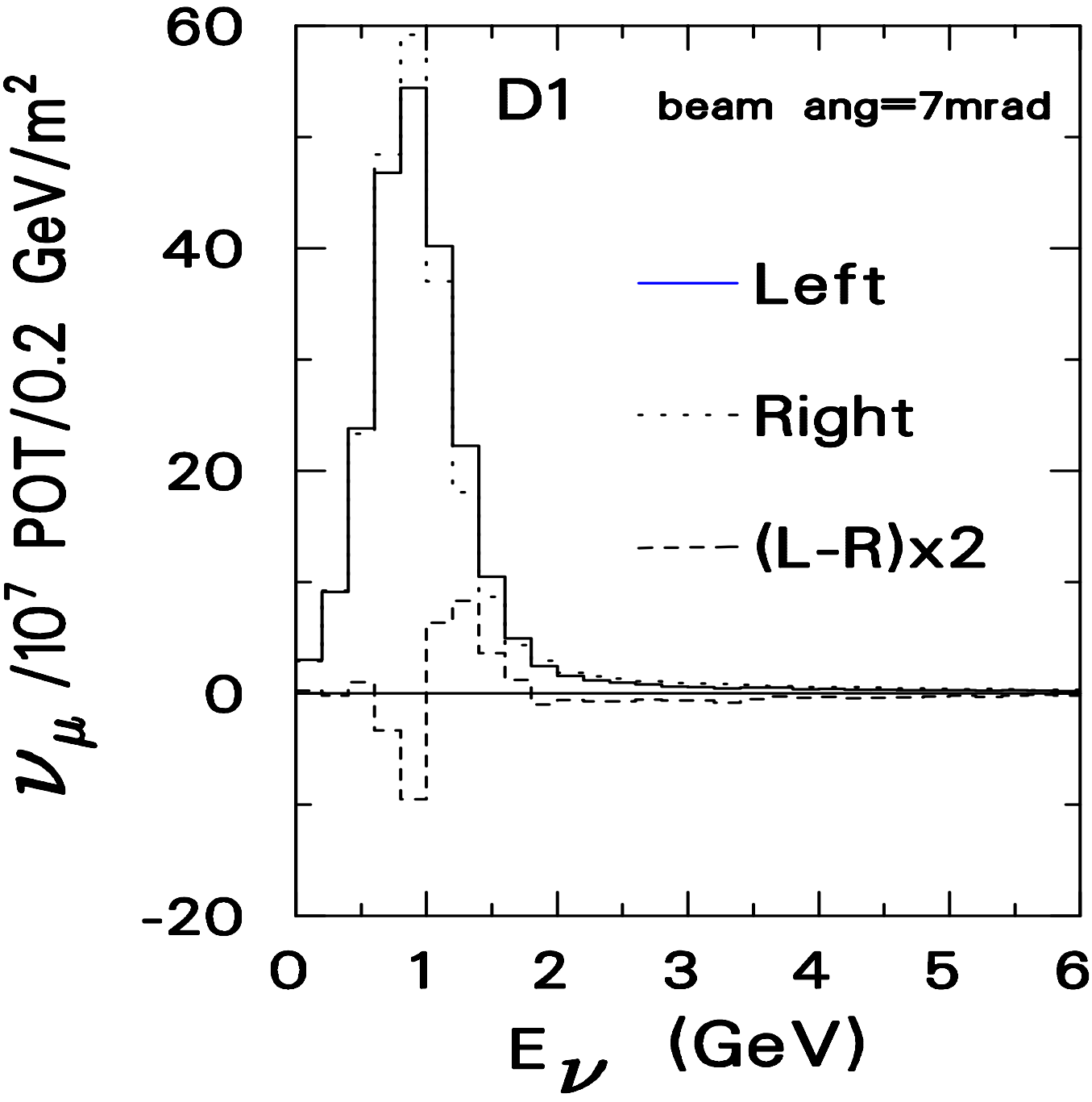
D1
beam ang=7mrad
Left
Right
(L-R)x2
60
40
20
0
-20
0
1
2
3
4
5
6
ν_μ /10^7 POT/0.2 GeV/m^2
E_ν (GeV)

Figure 14

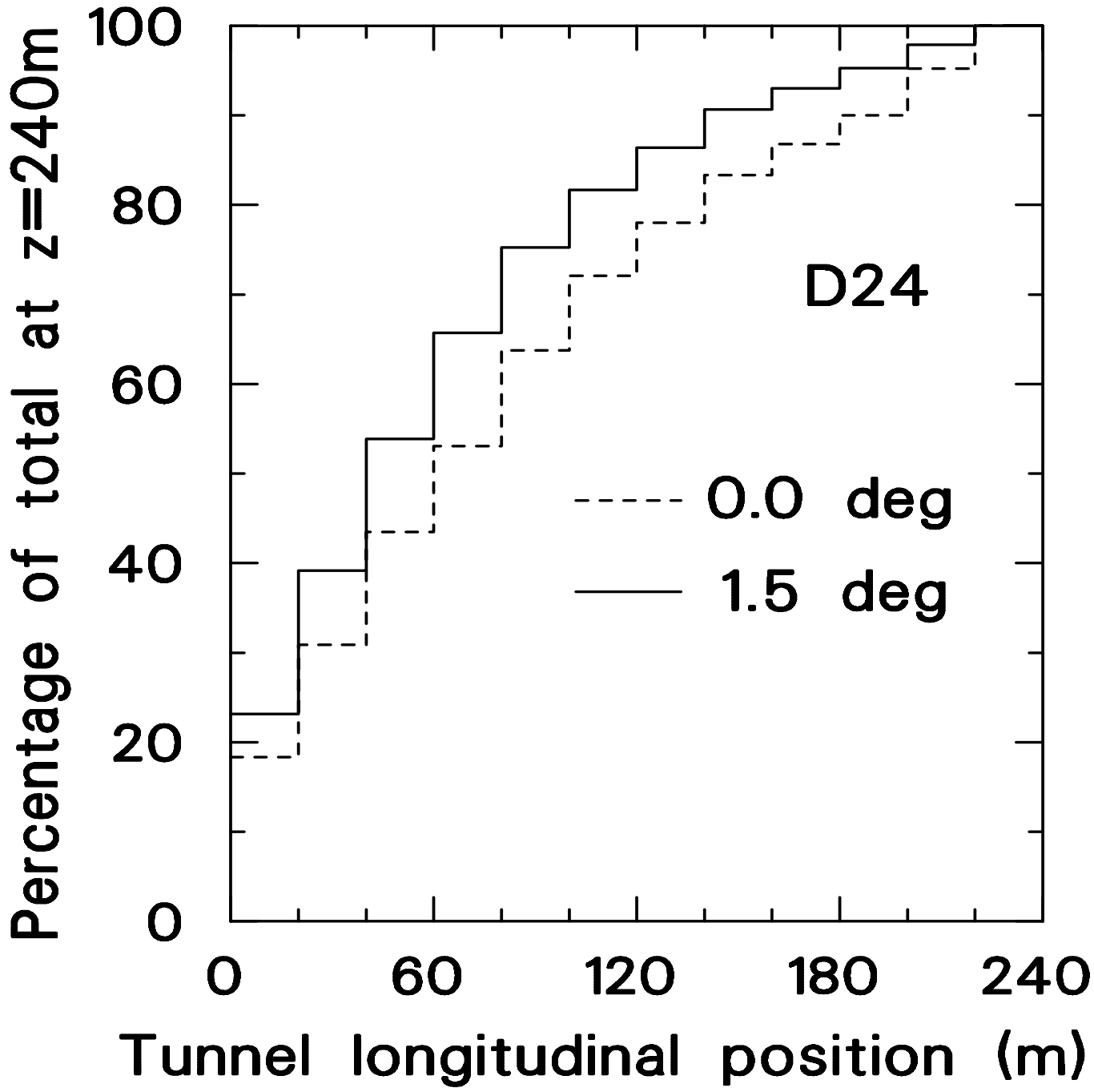
Percentage of total at z=240m
100
80
60
40
20
0
0
60
120
180
240
Tunnel longitudinal position (m)
D24
0.0 deg
1.5 deg

Figure 15

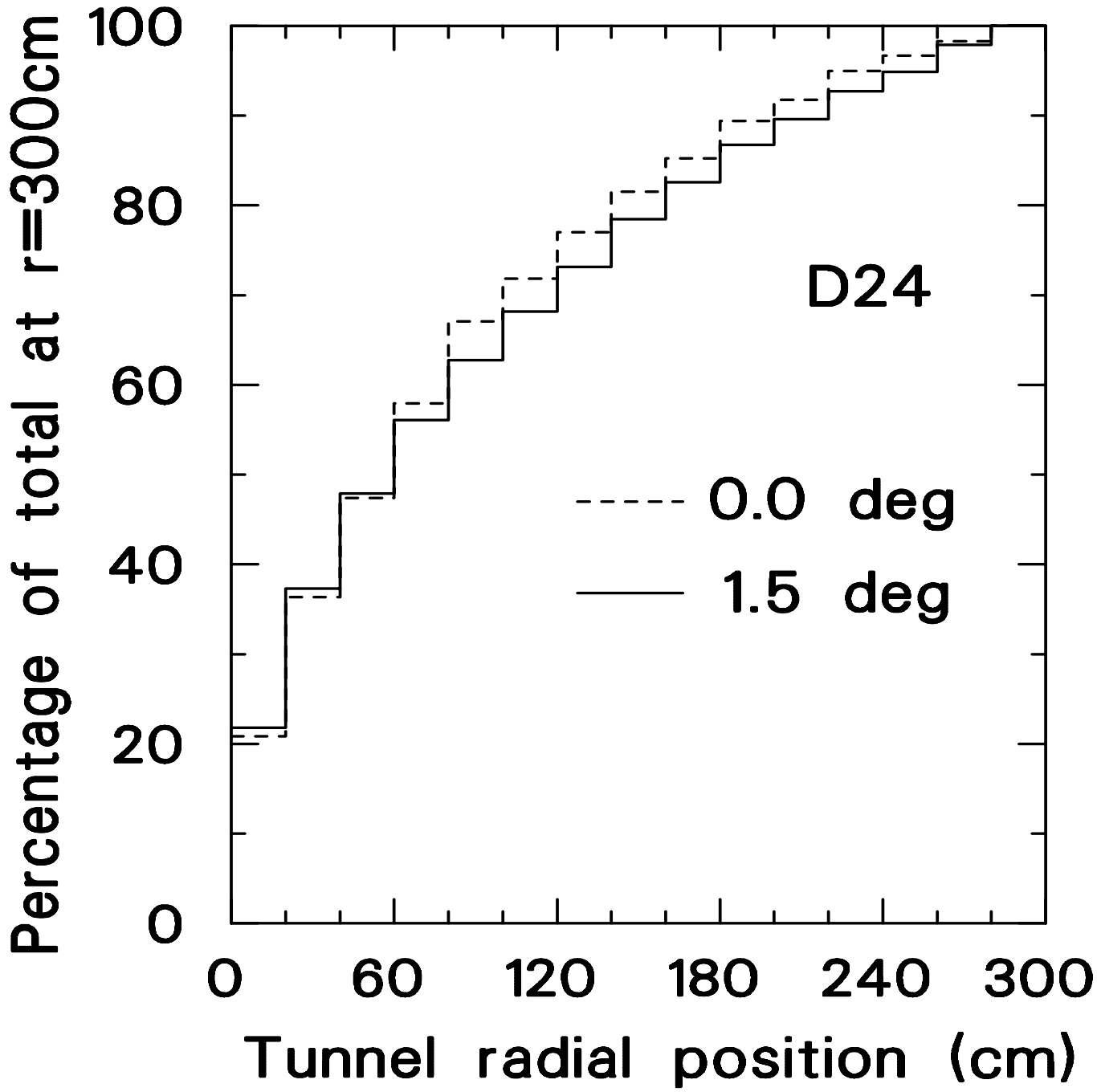
Percentage of total at r=300cm
100
80
60
40
20
0
0
60
120
180
240
300
Tunnel radial position (cm)
D24
0.0 deg
1.5 deg

Figure 16

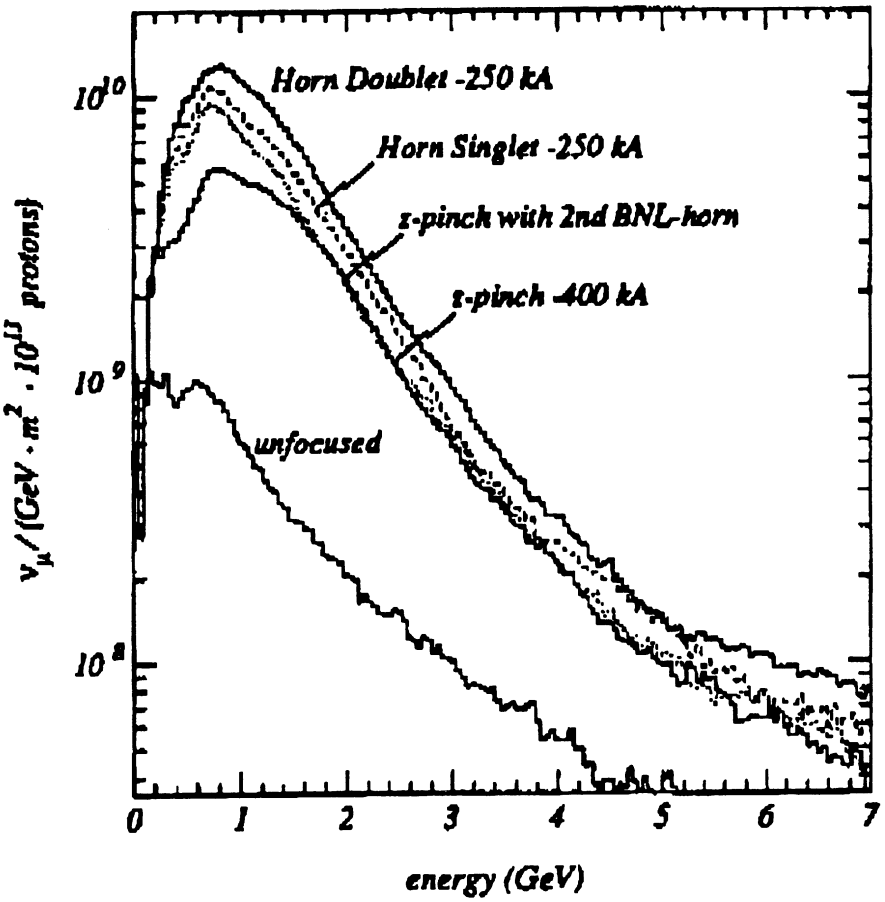
Horn Doublet -250 kA
Horn Singlet -250 kA
z-pinch with 2nd BNL-horn
z-pinch -400 kA
unfocused
10^{10}
10^{9}
10^{8}
ν_μ/[GeV · m^2 · 10^{15} protons]
0
1
2
3
4
5
6
7
energy (GeV)

Figure 17

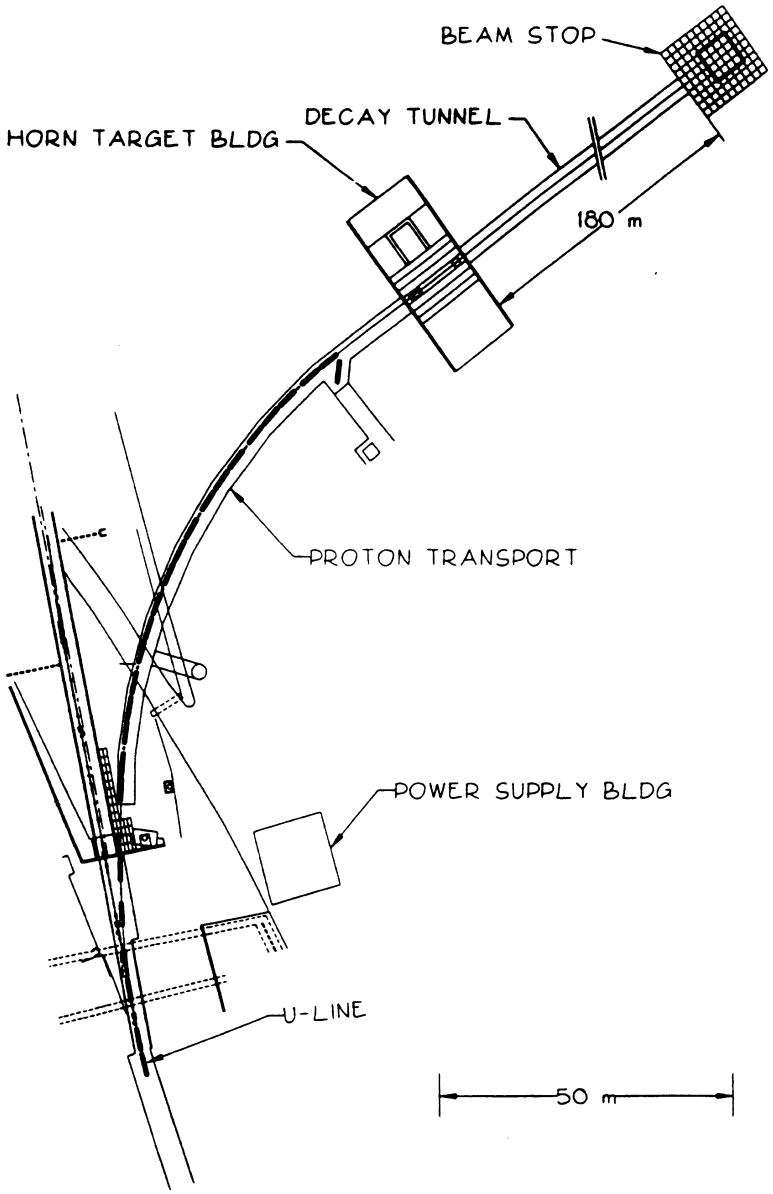
BEAM STOP
DECAY TUNNEL
HORN TARGET BLDG
180 m
PROTON TRANSPORT
POWER SUPPLY BLDG
U-LINE
50 m

Figure 18

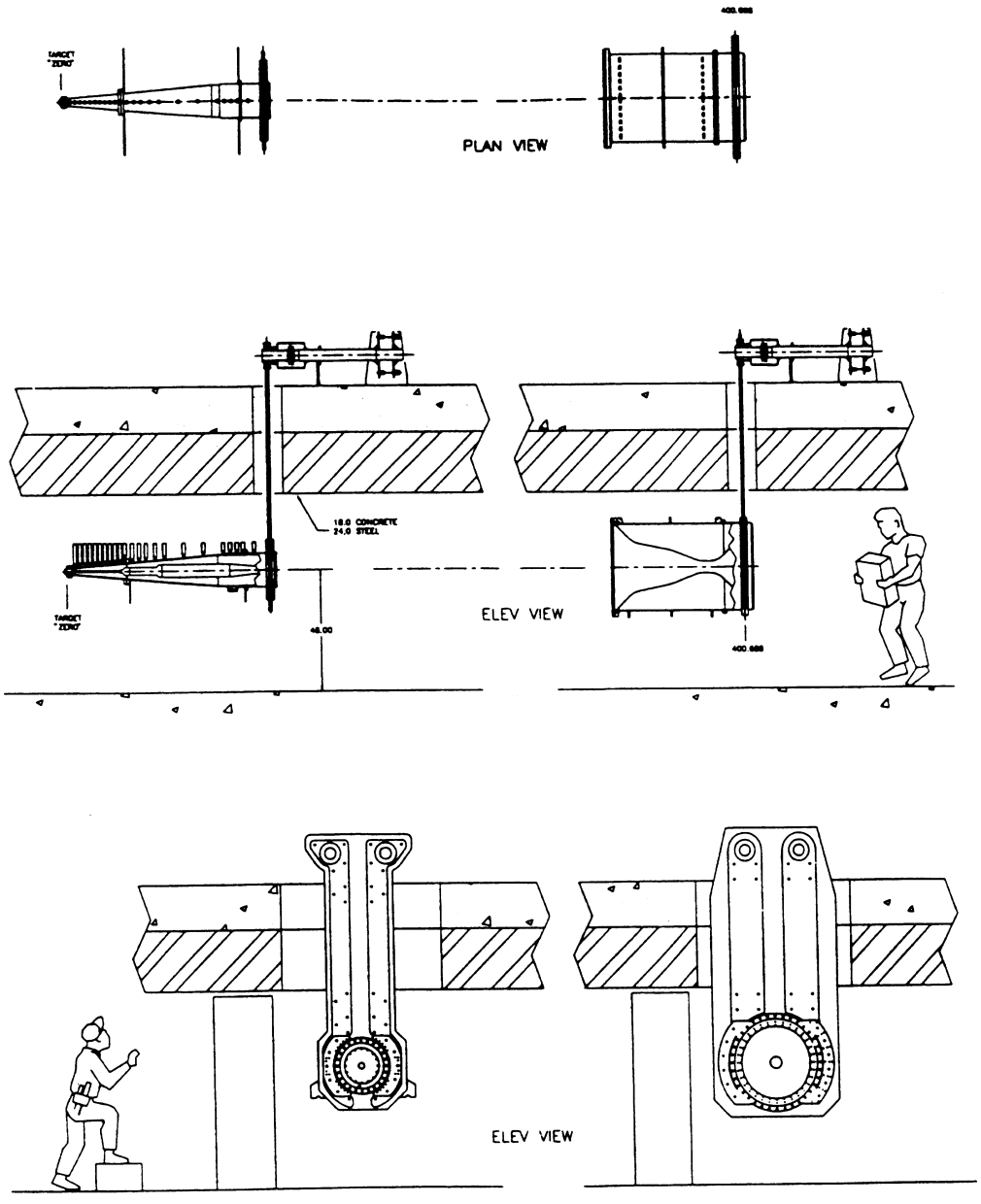

Figure 19

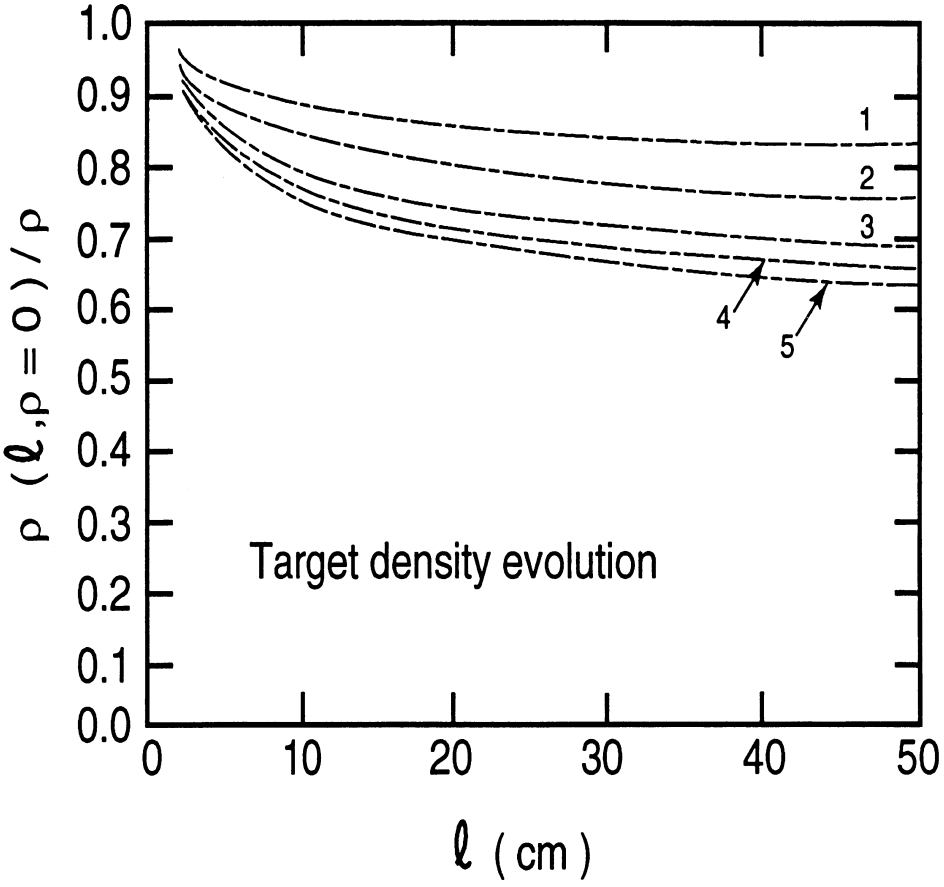
1.0
0.9
0.8
0.7
0.6
0.5
0.4
0.3
0.2
0.1
0.0
ρ (ℓ,ρ = 0) / ρ
0
10
20
30
40
50
ℓ (cm)
1
2
3
4
5
Target density evolution

Figure 20

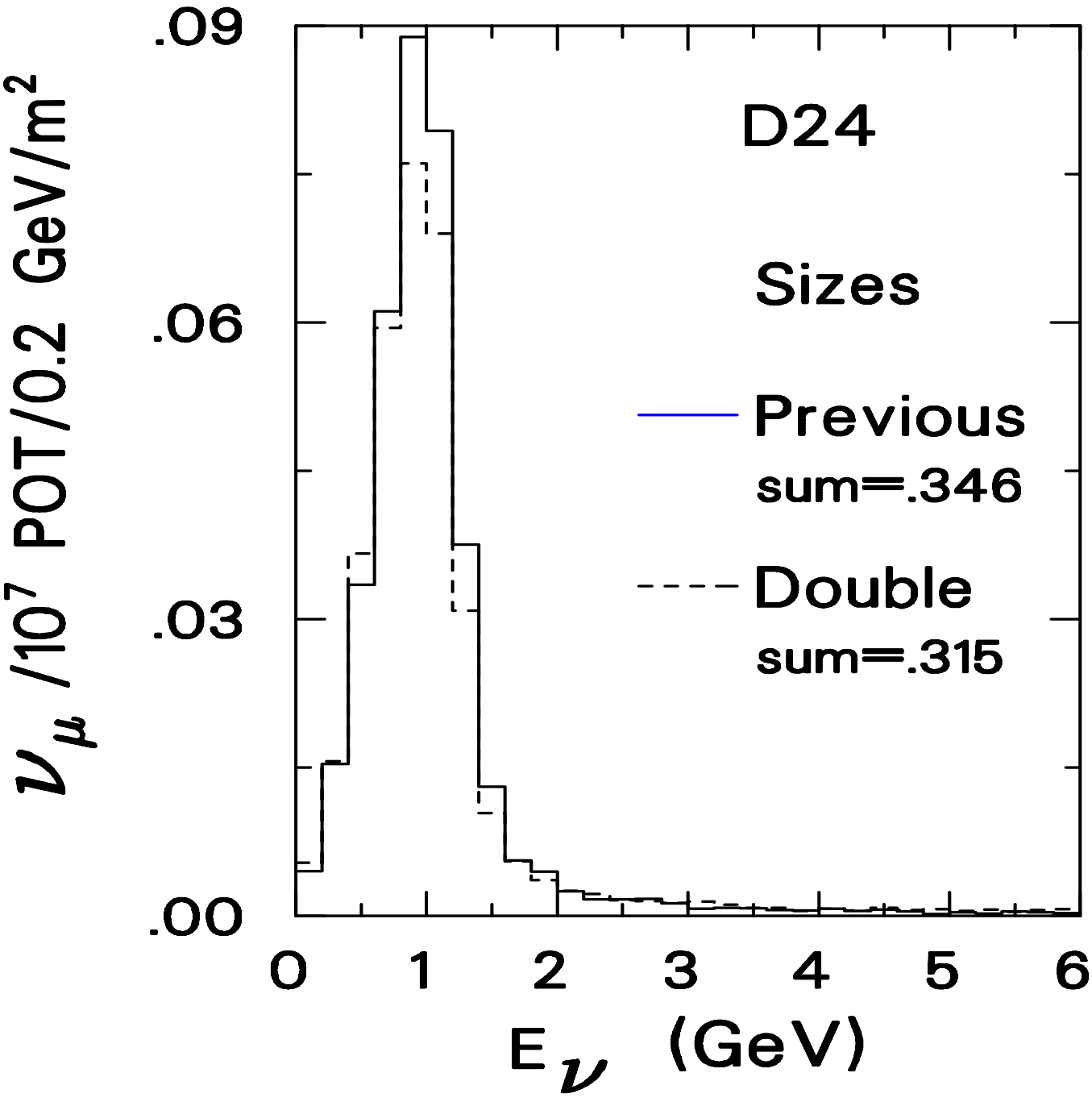
.09
.06
.03
.00
ν_μ /10^7 POT/0.2 GeV/m^2
D24
Sizes
Previous
sum=.346
Double
sum=.315
0
1
2
3
4
5
6
E_ν (GeV)

Figure 21

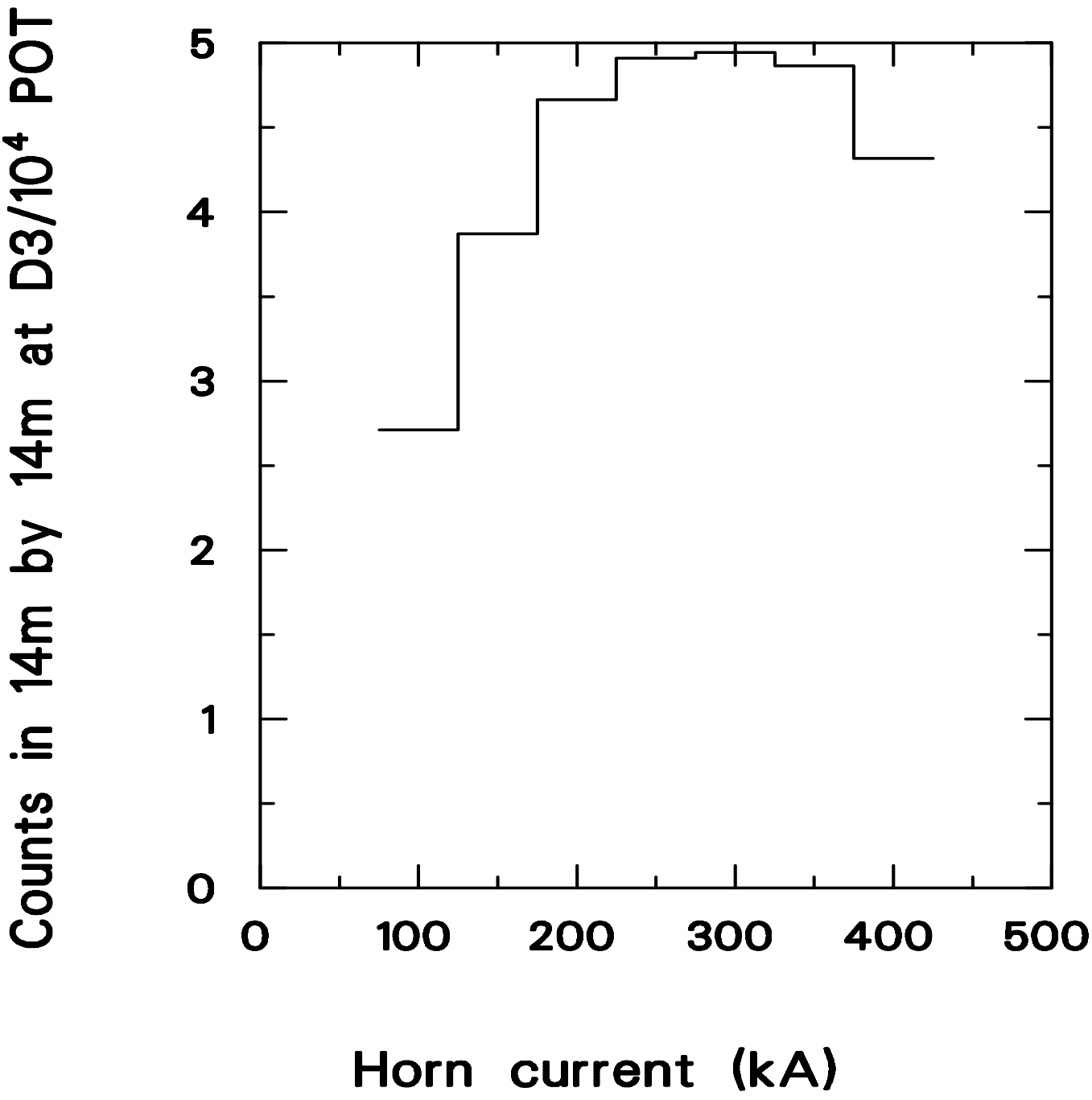
Counts in 14m by 14m at D3/10⁴ POT
0
1
2
3
4
5
0
100
200
300
400
500
Horn current (kA)

Figure 22

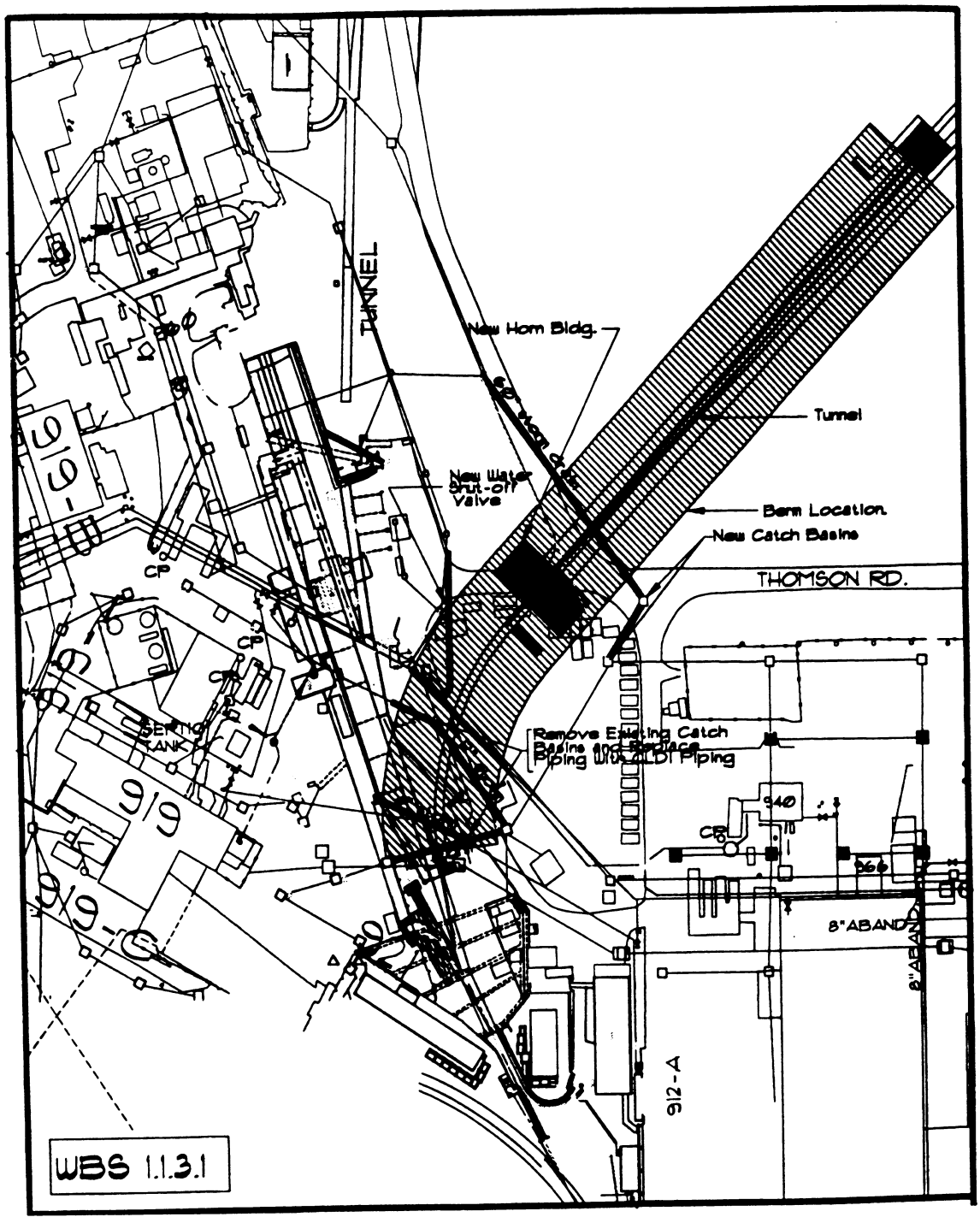
TUNNEL
New Horn Bldg.
Tunnel
New Water Shut-off Valve
Berm Location
New Catch Basins
THOMSON RD.
CP
CP
SEPTIC TANK
Remove Existing Catch Basins and Replace Piping with DI Piping
940
CB
966
8"ABAND
8"ABAND
912-A
WBS 1.1.3.1

Figure 23